MASTER

Bacterial motility and deposition patterns in evaporating drops with a pinned contact line

van Bunder, T.M.L.A.

Award date:
2019

UNIVERSITY OF TECHNOLOGY EINDHOVEN

MASTER THESIS

Bacterial motility and deposition patterns in evaporating drops with a pinned contact line

R-1995-A

Author:
Terry van Bunder

Supervisor:
Hanneke Gelderblom

A thesis submitted in fulfillment of the requirements for the degree of Master Thesis

in the

Turbulence and Vortex Dynamics
Applied Physics

September 5, 2019

Acknowledgements

At the end of this challenging research, I would first and foremost like to thank Hanneke Gelderblom for all her guidance, advice, stern questions and friendly attitude. I would like to thank Anton Darhuber and Federico Toschi for their additional guidance, on experimental issues and theoretical insights, respectively. I would like to thank Ad Holten for numerous help with software issues, such as his work on test data; and Jorgen van der Veen for (de-)constructing the setup. I would like to thank Alvaro Marin and Rune Barnkob for help with particle tracking software. I would like to thak my colleague students such as Gerben Beintema and Twan Wilting for their insights and companionship; and finally I would like to wish Hanneke and Twan success for contuining the research.

...

Contents

Chapter 1

Abstract

Evaporating drops have received wide attention as method of creating well-defined microscopically sized structures from the deposited colloids that form into a ring-shaped "coffee-stain". Using self-propellant particles or bacteria can show interesting new deposition patterns that may have applications in fields such as biotechnology, tissue engineering and small-scale bio-medical diagnostics.

In this paper we examine the effect of particle motility on the deposition pattern, by comparing particle velocity and deposition pattern of motile and non-motile E.Coli bacteria to test measurements with polystyrene colloidal particles. A two-dimensional version of General Defocused Particle Tracking (GDPT) was used to track the particles. Our observations show that a nonzero salt concentration in a motility buffer solution may give rise to additional flows or additional structure formation in the deposition pattern.

The motile E. Coli bacteria appear to move out of the contact line deposition unless stuck between other bacteria or the wedge-shaped contact line region. Over time, motility decreases, such that the bacteria act as passive tracers. The decrease in motility and fluorescence has important implications for research into bacteria-laden evaporating drops, suggesting cell injury. Though it has not been possible to investigate bacterial motion in the final stages of evaporation, our results hint to interesting contact line region behavior of motile bacteria.

Chapter 2

Introduction

Bacteria-laden drops are ubiquitous in the world, but also have a wide variety of applications in technology fields ranging from bio-technology and tissue engineering to medicine fabrication. In all these applications, it is important to understand how bacteria suspended in liquid drops get deposited. Conversely, the contamination caused by spreading bacterial colonies may be understood better, such that the cleaning of hospitals and cleanrooms may benefit from a better understanding of the deposition of bacteria in evaporating drops.

A myriad of phenomena occur in bacteria-laden evaporating drops, which have varying hydrodynamical, chemical and biological properties. The fluid motion induced by swimming bacteria can for example cause convection, decrease viscosity or lead to microscale mixing (Dombrowski et al., 2004; Yeomans, Pushkin, and Shum, 2014; Kasyap, Koch, and Wu, 2014b; Koch and Subramanian, 2011). The formation of biofilm drastically changes properties of the fluid and response of bacteria to changes in the environment, generally enhancing bacterial durability.

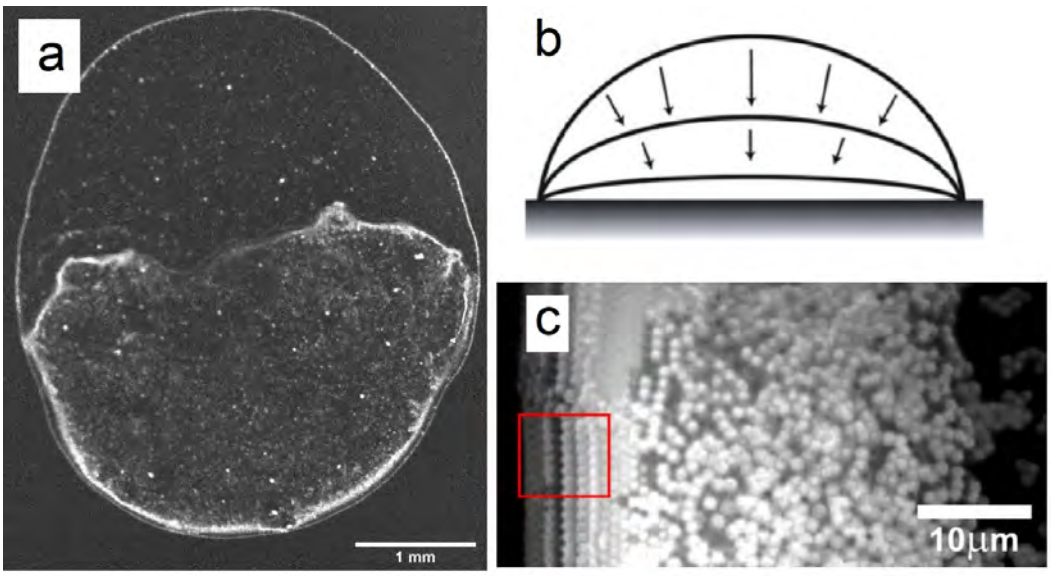

FIGURE 2.1: (a) Deposition pattern of water drop containing fluorescent passive colloids, forming a ring-shape "coffee-stain" pattern. (b) Schematic representation of evaporating drop with pinned contact line (Figure by (**Parsa2018**). (c) Deposition pattern of colloids in drop after evaporation showing well-ordered structure (left, red box) and disordered packing (right) (Figure by (Marin et al., 2011)

.

Unlike passive colloids that are passively transported by the imposed flow and deposit into a commonly known "coffee-stain" ring pattern such as shown in Figure 2.1, bacteria are individually moving, self-propellant organisms that may show different movement (Deegan et al., 1997a; Lauge and Powers, 2009). Their direction of movement is attuned to concentration gradients in the medium as they search for nutrients or oxygen, a process called chemotaxis (Kasyap and Koch, 2012; Dombrowski et al., 2004). Bacterial movement is also sensitive to proteins excreted by other bacteria within a population, which indicates a form of communication between bacteria that may even lead to programmed cell death within individual bacteria to ensure the population's prolonged existence.

E.Coli bacteria are commonly used as a model active colloid in research (Schwarz-Linek et al., 2016). E.Coli bacteria show a "run and tumble" movement in which they move forward in a straight line and reorient with sharp turns (Lauge and Powers, 2009; Yeomans, Pushkin, and Shum, 2014). E.Coli can also be genetically modified to portray different movement. Examples of this are continuously tumbling or continuously moving forward E.Coli to isolate velocity components, or E.Coli showing no movement at all to investigate chemical or biological effects on the drop or flow that the bacteria may have.

Collective behavior such as collective bacterial motion and self-assembly have been observed to occur in various configurations, due to for example chemotaxis-driven or evaporation-driven accumulation of bacteria (Kasyap, Koch, and Wu, 2014b; Koch and Subramanian, 2011; Dombrowski et al., 2004). In a slowly evaporating drop, bacteria swim towards the top of the drop surface in search of oxygen and slide down towards the contact line, thereby acquiring high concentrations and showing large-scale dynamic coherence in the form of bacterial jets that show movement an order of magnitude larger than individual motion and vortices (Dombrowski et al., 2004) such as shown in Figure 2.2. Similar jets have been observed to form due to the evaporation-driven radially outward flow in a evaporating sessile drop with pinned contact line (Kasyap, Koch, and Wu, 2014a).

Though research has investigated bacterial motion in evaporating drops, little attention has been given to the fundamental interaction between actively moving bacteria and contact line dynamics, without collective behavior or the added complexity of spontaneously generated bacterial motion.

The configuration of evaporating sessile drop with pinned contact line has been investigated widely and already reveals interesting phenomena with passive colloids (Deegan et al., 1997a; Marin et al., 2011). Since (Deegan et al., 1997a)'s pioneering work, various theoretical frameworks, numerical simulations and experimental studies have been used to investigate evaporating drops, the flows occurring within, and the deposition patterns that arise (Deegan et al., 1997a; Marin et al., 2011; Popov, 2005; Hu and Larson, 2005; Jaijus and Singh, 2010). Various analytical expressions for the evaporative flux have been derived, depending on the drop's geometry, composition, temperature gradients, substrate roughness, ambient humidity. For example, a drop on a cooled or heated substrate shows temperature-driven or a drop with non-zero salt concentration show Marangoni flows, surface-tension driven flows. Of particular interest in the literature is an evaporating sessile drop with pinned contact line.

Such a drop produces a radially outward capillary flow to replenish the evaporation-induced fluid deficit at the contact line (Deegan et al., 2000; Deegan et al., 1997b; Deegan et al., 1997a). This flow transports all colloids towards the contact line, thereby forming a ring-shaped stain that is more commonly known as the "coffee-ring" stain and is often used in fields of nanotechnology, printing, and biotechnology to create

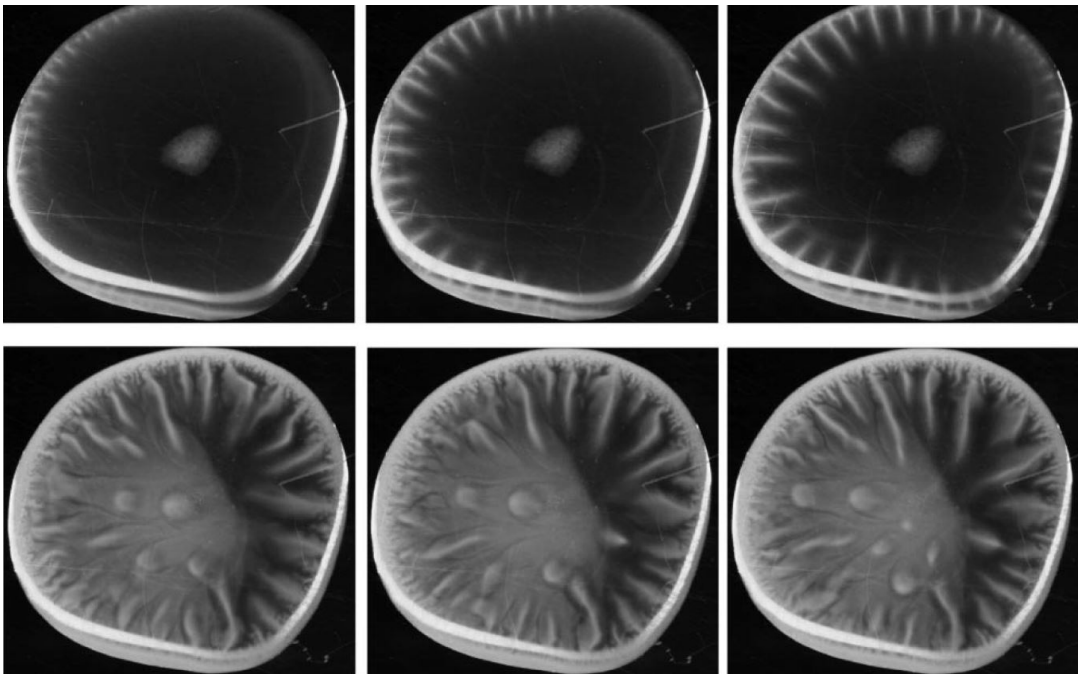

FIGURE 2.2: Contact line deposition with motile bacteria over time, forming finger-like jets towards the drop center due to self-generated large-scale motion (Figure by (Dombrowski et al., 2004)

.

ordered arrays of deposited colloidal particles. The colloids form into a well-ordered pattern at the contact line that transitions into a disordered array. (Marin et al., 2011) has revealed the cause of this transition to be the temporal and spatial singularity in the radially outward capillary flow. In other words, there is a direct link between deposition pattern and particle velocity induced by the flow, as hinted to by Deegan. However, how does this change if particles are self-propelled such as bacteria?

In particular, how do self-propagating E.Coli bacteria deposit in an evaporating drop and can this compared to the deposition of passive tracers?

In this work, we investigated how the evaporation-induced deposition pattern of solutes in a sessile drop is affected by self-propagating suspended particles. To this end, we tracked bacterial motion using Particle Tracking Velocimetry (PTV) by fluorescently labelling E.Coli bacteria. We compared results to the same experiment with colloidal particles of a similar size that act as passive tracers. Further, we compared the deposition patterns generated by motile and non-motile E.Coli strains with respect to the deposition patterns of passive colloids. In addition, we investigated the influence of the motility buffer solution that is used to perform measurements with bacteria.

Chapter 3

Theoretical background

The first section describes droplet evaporation and gives an expression for the evaporative flux. The second section describes how the evaporative flux of a drop with pinned contact line leads to a capillary radially outward flow. This flow drags passive suspended particles to the contact line. The deposition pattern that forms is explained in the third section. This pattern may form differently when particles are motile, such as self-propagating bacteria. The movement of a single bacterium is described in the fourth section and bacterial collective motion in the final section.

3.1 Drop evaporation

This section is split into two parts. The first subsection considers the evaporative flux and the second considers the change in drop shape that follows.

3.1.1 Evaporative flux

When the air is not fully saturated with vapor, a drop of fluid in contact with ambient air will evaporate (Deegan et al., 1997a; Marin et al., 2011; Rapp, 2016). During evaporation, liquid molecules from the drop leave from its surface into the surrounding air.

Diffusion of vapor away from the drop results from the difference in vapor concentration at the drop surface and far away from it, $c_v(1-H)$, where H is the humidity and c_v is the saturated vapor concentration. This difference in concentration is the driving factor for evaporation.

The spreading of vapour in the surrounding air can then be described with the diffusion equation, which is given by

$$\frac{\partial c}{\partial t} = D\Delta c, \tag{3.1}$$

in which c is the vapor concentration, D the diffusion constant and t the time (Deegan et al., 1997a; Popov, 2005; Marin et al., 2011).

At the drop surface, the air is saturated with vapor due to evaporation. The vapor concentration is then given by the saturation value c_v. The vapor-concentration adjusts to the change in drop shape in a time scale in the order of R^2/D with diffusivity D. This time can be compared to the time of evaporation t_e with the ratio $\frac{R^2/D}{t_e} \approx \frac{c_v}{\rho}(1-H)$ (Hu and Larson, 2002). With $c_v = 2.32x10^{-2} kg/m^3$, $\rho = 10^3 kg/m^3$ and H in the order of $O(1)$, this ratio is $O(10^{-5}) \ll 1$. In other words, the change in vapor concentration occurs much faster than the drop's shape change. As such, evaporation can be viewed as quasi-steady and Equation 3.1 thereby reduces to the

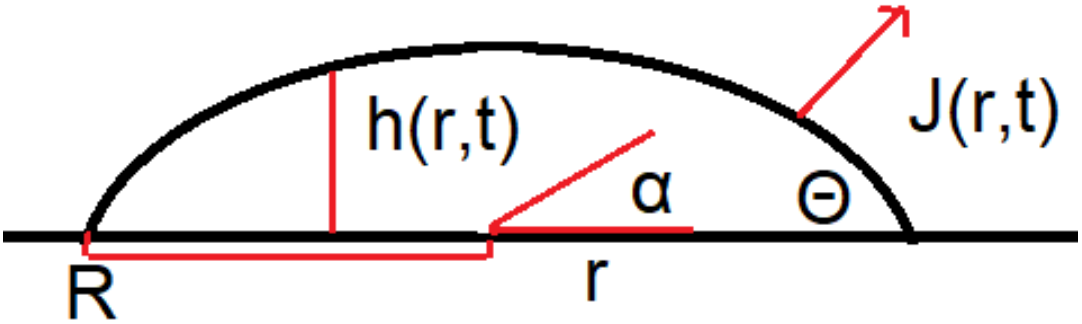

FIGURE 3.1: Schematic representation of the evaporating sessile drop in the axisymmetrical cylindrical coordinate system $(r, , \phi)$ with initial base radius R, parabolic height profile $h(r,t)$, evaporative flux $J(r,t)$, and contact angle $\theta(t)$.

Laplace equation

$$\Delta c = 0. \tag{3.2}$$

The configuration of a drop on a substrate is subject to the following boundary conditions (Deegan et al., 1997a; Hu and Larson, 2005). (1) The vapor concentration is a constant c_v along the drop surface, because the air is saturated with vapor just outside the drop. (2) The vapor concentration decreases to a constant $c_v(1-H)$ far from the drop. (3) The flux $-D\partial_n c$ is zero at the substrate surface, because no vapor penetrates into the substrate. Hence, these three boundary conditions read

$$c(r = R, \theta) = c_v \tag{3.3}$$

$$c(r \to \infty, \theta) = c_\infty \tag{3.4}$$

$$-D\partial_n c(r > R, \theta = 0, \pi) = 0 \tag{3.5}$$

,

considered in the axisymmetric cylindrical coordinate system (r, θ, ϕ), displayed in Figure 3.1. As can be seen, the origin is located in the center of the drop and the drop surface at $r = R$. The substrate constitutes the entire space described by $\pi << 2\pi$ where no vapour can penetrate. As such, the substrate can be seen as mirror plane (Deegan et al., 2000; Deegan et al., 1997b; Hu and Larson, 2005). The problem $2.2 - 2.7$ is similar to the problem of a similarly-shaped charged conductor in electrodynamics in which the substrate is taken as mirror plane. Near the contact line, the drop and its reflection form a wedge. For a small contact angle θ between drop surface and substrate, solving this configuration or copying the electrostatic analog gives an expression of (Deegan et al., 2000; Deegan et al., 1997b; Hu and Larson, 2005)

$$J(r) = \frac{2}{\pi} \frac{D_{va}\Delta c}{\sqrt{R^2 - r^2}}, \tag{3.6}$$

in which $D_{va} = 24x10^{-6} m^2/s$ is the diffusion constant of vapor in air, $\Delta c = c_v - c_\infty$ the difference in vapor concentration between the saturated value near the drop and the ambient value far away. This expression depends only on r, indicating that evaporation increases towards the contact line and is constant in time.

3.1.2 Change in droplet shape

Evaporation reduces the volume of the drop, resulting in a change of drop shape. The drop shape will be discussed presently, after which the change in shape can be discussed.

The shape of a drop is determined by the forces that work on it, e.g. the gravity force and surface tension . Surface tension curves the drop into a spherical shape. On the other hand, the drop is flattened by the effects of gravity.

The relative strength of these effects is characterized by the Bond number, or Eötvös number, $Bo = (\frac{L}{\lambda_c})^2$ (Hocking, 1983; Rapp, 2016). The length scale L is defined by the drop's radius of curvature, which is $h < 1mm$. The capillary length λ_c has a typical value of $3mm$ for a water drop at room temperature. These values give a Bond value smaller than one, indicating that surface tension dominates when compared to gravity (Li et al., 2018; Rapp, 2016).

In other words, when the contact line remains pinned during evaporation, the drop shape can be described by the parabolic approximation of a spherical-cap profile (Marin et al., 2011)

$$h(r,t) = \frac{R^2 - r^2}{2R}\theta(t), \tag{3.7}$$

with contact angle $\theta(t)$. The contact angle can be determined from the rate of mass lost from the drop, which is determined by the total evaporative flux.

The total amount of evaporated fluid is given as

$$\frac{dV}{dt} = \frac{1}{\rho}\int JdA = -\frac{1}{\rho}\int_0^R J(r,t)2\pi r dr \tag{3.8}$$

$$= -\frac{1}{\rho}\int_0^R \frac{2}{\pi}\frac{D_{va}\Delta c}{\sqrt{R^2 - r^2}}2\pi r dr \tag{3.9}$$

$$= -\frac{4RD\Delta c}{\rho} \tag{3.10}$$

Conversely, the change in droplet volume can be written as

$$\frac{dV}{dt} = \frac{1}{\rho}\frac{dM}{dt} = \frac{d}{dt}\int_0^R h(r,t)2\pi r dr \tag{3.11}$$

$$= \frac{d}{dt}\int_0^R \frac{R^2 - r^2}{2R}\theta(t)2\pi r dr \tag{3.12}$$

$$= \frac{\pi R^3}{4}\frac{d\theta}{dt}. \tag{3.13}$$

Equating these and solving for $\theta(t)$ gives an expression for $d\theta/dt$ that is independent of time. As such, it can be integrated directly to give

$$-\frac{4RD\Delta c}{\rho} = \frac{\pi R^3}{4}\frac{d\theta}{dt}. \tag{3.14}$$

$$\frac{d\theta}{dt} = -\frac{16D\Delta c}{\pi R^2 \rho} \tag{3.15}$$

$$\theta(t) = -\frac{16D\Delta c}{\pi R^2 \rho}(t_e - t), \tag{3.16}$$

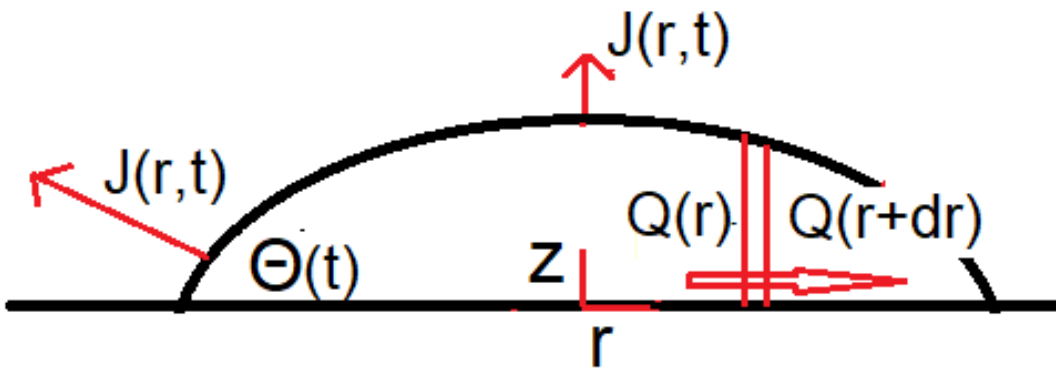

FIGURE 3.2: Schematic representation of the evaporating sessile drop in the cylindrical coordinate system (r, z) with evaporative flux $J(r, t)$ that increases towards the contact line, $Q(r), Q(r + dr)$ and contact angle $\theta(t)$.

in which t_e is the total time of evaporation. The evolution of height and contact angle over time now are given as Equations 3.7 and 3.1 respectively.

When the contact line remains pinned during evaporation and the drop's radius remains constant, the Equations above holds (Deegan et al., 1997a; Marin et al., 2011). Equation 3.16 shows that the contact angle decreases linearly over time. With the constant radii, Equation 3.7 shows that the height changes with a similar linear decrease over time.

However, when the contact line depins, these expressions and assumptions are not valid. During depinning, the contact line retreats towards the center such that the contact angle once more attains the equilibrium angle for which the surface tension is lowest (Parsa, Harmand, and Sefiane, 2018).

When fluid leaves the drop due to evaporation, its shape needs to change to accommodate this volume loss. For a drop with pinned contact line, the change in drop shape is the result of a decreasing height and contact angle. As such, the decrease in volume is highest at the top of the drop and lowest at the contact line (Deegan et al., 1997a; Popov, 2005; Hu and Larson, 2005; Marin et al., 2011).

However, this volume decrease does not match the volume taken away by evaporation, which is explained to be lowest at the top of the drop and highest at the contact line. Evidently, there is a volume deficit at the contact line and a surplus at the top. If the configuration of a drop with pinned contact line is to persist, a mechanism needs to arise that replenishes volume lost at the edge from the surplus volume at the top. In other words, a radially outward capillary flow arises.

An expression for this flow is derived below using mass conservation. Figure 3.2 shows the axisymmetric drop with pinned contact line that is described in a cylindrical coordinate system (r, z). An infinitesimally small control volume of width dr is defined at a distance r from the drop center. Inside this control volume, the change in drop height is equal to the rate of change of the amount of liquid inside. Local mass conservation dictates that this change is equal to the sum of the net inflow of liquid into the control volume and the amount of liquid evaporated from the drop surface.

3.2 Passive flow inside drop

Without evaporation, the local change in drop height due to any flow can be written as

$$\rho \frac{\partial h}{\partial t} = \frac{Q_r - Q_{r+dr}}{dr} = -\frac{1}{r}\frac{\partial Q}{\partial r}, \tag{3.17}$$

with $h(r,t)$ the local drop height and $Q(r,t)$ the volume flow through the control volume.

The amount of evaporated fluid is given by the multiplication of the evaporative flux $J(r,t)$ and the surface area dS. For the small drop under consideration, it holds that $dS = \sqrt{1 + (\frac{\partial h}{\partial r})^2}$. The term $\frac{\partial h}{\partial r}$ is small over the entire drop surface and $(\frac{\partial h}{\partial r})^2$ can be considered negligible compared to 1, giving $dS = dr$. Taking these elements together, the local mass conservation reads (Deegan et al., 2000)

$$\rho \frac{\partial h}{\partial t} = -\frac{\rho}{r}\frac{\partial}{\partial r} Q - J. \tag{3.18}$$

Taking Equations 3.7 and 3.15 together into the local mass conservation of Equation 3.18 gives, by integration, an expression for the volume flow

$$Q(r) = \frac{2D_{va}\Delta c}{\pi\rho}\left(\sqrt{R^2 - r^2} - \frac{1}{R^3}(R^2 - r^2)^2\right) \tag{3.19}$$

For any flow through a certain surface, the volume flow Q is equal to the surface area times the velocity averaged over the surface. Here, the averaged velocity is the height-averaged velocity $\bar{u}(r,t)$. In other words, the volume flow can be written as

$$Q(r,t) = 2\pi r h(r,t)\bar{u}(r,t), \tag{3.20}$$

in which $\bar{u}(r,t)$ is the height-averaged velocity and $h(r,t)$ the height as given before. Solving for the velocity and linearizing for $r \to R$, near the contact line, gives

$$\bar{u}(r,t) = \frac{2\sqrt{2}D_{va}\Delta c}{\pi\rho\sqrt{R}}\frac{1}{\theta(t)}\frac{1}{\sqrt{R^2 - r^2}}. \tag{3.21}$$

The factor $D^* = \frac{2\sqrt{2}D_{va}\Delta c}{\pi\rho}$ can be recognized as a constant that, together with the shape constraint imposed by surface tension, drives the flow (Deegan et al., 1997a; Popov, 2005).

This height-averaged velocity is dissimilar to experimental observations of particle velocity at a small distance above the substrate(Marin et al., 2011). This discrepancy is caused by the no-slip boundary condition of the substrate, dictating that the flow velocity declines to zero at the substrate. Prompted by these observations, a height-dependent velocity profile $u(r,z,t)$ has been derived.

To this end, the Navier-Stokes is simplified. Due to low velocities ($O(10\mu m/s)$) and hence low Reynolds number, the inertial terms are negligible. Due to the small contact angle, the drop has a small height-to-radius ratio $H/R << 1$. From the continuity equation, it then holds that velocity in the vertical direction is negligibly small compared to velocities in the horizontal direction, since $U/V\ R/h >> 1$. The lubrication approximation then holds, such that the Navier-Stokes equations can be

reduced to (Marin et al., 2011; Oron, Davis, and Bankoff, 1997)

$$\frac{dp}{dr} = \mu \frac{\partial^2 u}{\partial z^2}, \tag{3.22}$$

in which $p(r)$ is the pressure, μ the dynamic viscosity and $u(r,z)$ the radial velocity.

This expression hints towards a velocity profile parabolic in height: $u(r,z) = a(r)z^2 + b(r)z + c(r)$. The constants can be determined by recognizing the no-slip and no-shear stress boundary conditions.

No-shear stress implies that on the liquid-air interface which is given by the drop profile $h(r,t)$, it holds that $\frac{\partial u}{\partial z} |_{z=h(r,t)} = 0$. No-slip implies that on the solid-liquid interface on the substrate, it holds that $u(r < R, 0) = 0$. Solving then gives

$$u(r,z) = \frac{1}{\mu}\frac{dp}{dr}\left(\frac{1}{2}z^2 - h(r,t)z\right), \tag{3.23}$$

which is dependent on height, pressure, and dynamic viscosity (Marin et al., 2011).

The pressure gradient can be exchanged for the height-averaged velocity, which has been given as Equation 3.21. Averaging 3.23 over the height gives $\bar{u}(r,t) = -\frac{1}{3\mu}\frac{dp}{dr}h^2(r,t)$, which can be rewritten to give the pressure gradient as function of the height-averaged velocity. The radially outward velocity is then finally given as

$$u(r,z,t) = \frac{3}{h^2(r,t)}\bar{u}(r,t)\left(h(r,t)z - \frac{1}{2}z^2\right), \tag{3.24}$$

in which $h(r,t)$, $\bar{u}(r,t)$ and $\theta(r,t)$ have been given by Equations 3.7,3.21 and 3.15, respectively. Repeated for good measure:

$$h(r,t) = \frac{R^2 - r^2}{2R}\theta(t) \tag{3.25}$$

$$\bar{u}(r,t) = \frac{2\sqrt{2}D_{va}\Delta c}{\pi\rho\sqrt{R}}\frac{1}{\theta(t)}\frac{1}{\sqrt{R^2 - r^2}}. \tag{3.26}$$

$$\frac{d\theta}{dt} = -\frac{16D\Delta c}{\pi R^2 \rho}, \tag{3.27}$$

with a contact angle that decreases linearly over time. The drop height is assumed to be parabolic and scales with contact angle, thereby also decreasing linearly over time. The height-averaged velocity shows a temporal and spatial divergence, increasing asymptotically when approaching the evaporation time or near the contact line.

The evaporative flux has a divergence in space; and the velocity profile shows divergent behavior in both space and time (Deegan et al., 1997a; Marin et al., 2011). This may be made clear by viewing Equation 3.24. It can be seen that the flow velocity depends inversely on $h(r,t)$ and consequently on $\theta(r,t)$. The contact angle approaches zero at the end of the evaporation time for a drop with pinned contact line. Evidently, the velocity increases over time and diverges near the end of the evaporation time due to the shrinking contact angle. Equations 3.24 and 3.21 show a spatial divergence that occurs near the contact line, for $r \to R$ due to the denominator in $1/\sqrt{R^2 - r^2}$ approaching zero.

The height-averaged velocity and complete velocity profile inside the evaporating drop are now given by Equations 3.21 and 3.24 respectively. These are plotted in

Figure 3.3. The velocity profile is plotted for two different heights. Due to the no-slip condition at the substrate, the velocity is lowest at the lowest height.

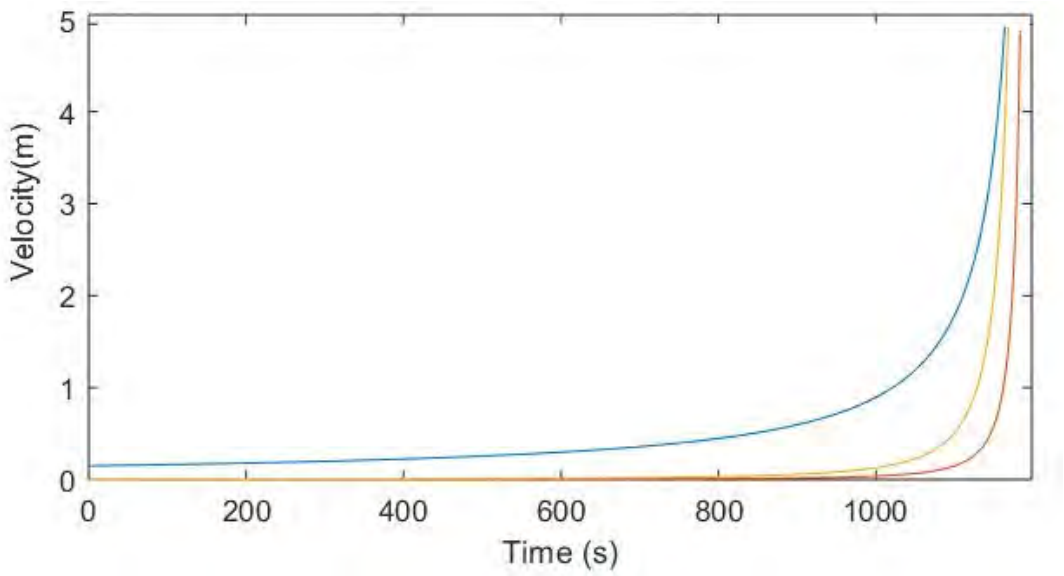

FIGURE 3.3: Theoretically expected radially outward flow in a sessile drop with pinned contact line, showing the height-averaged velocity (blue), velocity profile at $z = 2\mu m$ (red) and $z = 10\mu m$ (yellow).

3.3 Stain formation

Up to this point, it has been implicitly assumed that all of the fluid flowing towards the contact line leaves the drop by evaporation. However, dispersed colloidal particles remain inside the drop. Colloidal particles that passively follow the flow are thereby dragged towards where most of the fluid leaves the drop, which is near the contact line.

In other words, colloidal particles deposit at the contact line, thereby forming the well-known ring-shaped coffee stain pattern. Pattern formation has been shown to change over time (Marin et al., 2011).

Early in drop evaporation, the amount of depositing particles is low due to the small flow towards the contact line. Particles are not completely motionless, but oscillate due to random Brownian motion [1]. This motion causes particles to arrange themselves into the configuration that takes up the least amount of space, unhindered by the particles that follow. Particles thereby form an ordered pattern.

However, as the flow increases asymptotically towards the end of evaporation, the amount of particles increases. These particles have no time to arrange themselves before being locked into place by the particles that follow, thereby forming a

[1] To express the random Brownian motion in terms of velocity; the Einstein-Smoluchowski equation calculates the mean displacement of a particle moving due to random Brownian motion (Islam, 2004). Derivation with respect to time gives the velocity

$$v_B = \sqrt{< \Delta x^2 >}/t = \sqrt{2D/t}, \tag{3.28}$$

with Δx the averaged net displacement, D the diffusivity of the colloids, and t the amount of time, taken as the intermittent time between subsequent frames as $1/fr$.)

disordered pattern (Marin et al., 2011). Since particles rush towards the contact line during this period, this phenomenon has been called the rush hour behavior.

In other words, the steep increase in velocity over time causes a transition in the deposition pattern from order to disorder.

However, several other deposition patterns may occur if the contact line depins or recedes (Parsa, Harmand, and Sefiane, 2018). For example, the contact line may depin towards a new position before the rush hour behaviour starts. Then it can be expected that the stain formed at the initial contact line position forms only an ordered pattern. If the contact line recedes continuously, the radially outward flow does not arise and the particles deposit randomly.

The occurrence of deposition patterns of passive colloids has been researched widely. However, how the pattern may change when particles are self-motile has received less attention.

To further investigate the pattern formation with E.Coli bacteria, first bacterial motion will be discussed.

3.4 Bacterial motion

Bacterial motion takes place at small length scales $O(10^{-9}m)$ and small velocity scales $O(10^{-8}m/s)$ where the Reynolds number $Re = \rho u L/\mu$ is very small, where ρ is the density, u the velocity scale, L the length scale and μ the dynamic viscosity of the fluid (Koch and Subramanian, 2011; Lauge and Powers, 2009; Schwarz-Linek et al., 2016; Yeomans, Pushkin, and Shum, 2014). The Reynolds number is the ratio of inertial and viscous forces. For bacterial motion, the inertia-driven terms in the Navier-Stokes equations are considered negligibly small compared to the viscous terms. In other words, the Stokes flow applies, similar to Equation 3.22.

Inertia is used by swimmers at larger scales to glide forward between strokes, allowing them to use strokes that are reversible in time. However, such strokes do not work on small scales.

Due to the negligible inertia, motion of a particle only occurs when a force is exerted on it. Motion halts immediately after the forcing stops, preventing the particle from gliding forward. A reversible stroke then moves the particle back to where it was, a problem that is also known as the Scallop theorem.

Evidently, bacteria require a special form of movement that is non-reversable in time.

Bacteria have two distinct ways of propagating themselves forward (Lauge and Powers, 2009). Some bacteria have appendages with which they pull themselves forward using the viscous fluid in front of them, such as the algae Chlamydomonas. Other bacteria have flagella that push the fluid behind them away, such as E.Coli. The former are known as pullers and the latter as pushers, which are considered here. Both are shown in Figure 3.4. As can be seen, these produce different velocity fields in the surrounding fluid.

The movement of pushers is determined by their moving tails, or flagella. These flagella can alternately wind up and unwind. Unwinded flagella produce undirected forcing that rotates the bacterium, which is called a 'tumble'. Winded flagella exert directed motion, causing the bacterium to move forward in a 'run'. Due to imperfections in the flagella, bacteria may curve slightly during a run, which is called rotary diffusion.

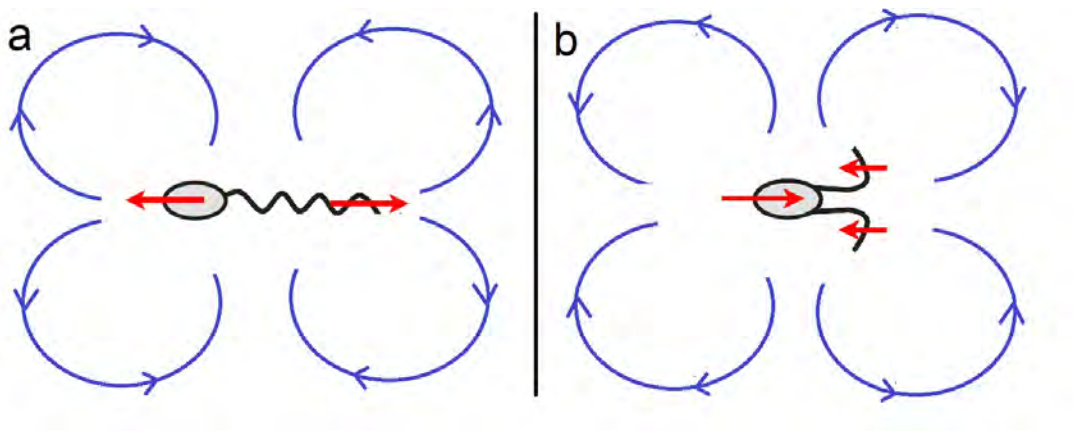

FIGURE 3.4: Schematic representation of a 'pusher' bacterium (a) and 'puller' bacterium (b). Pushers repel fluid along the direction they are facing. Along the axis parallel to the body, these pushers repel fluid. Perpendicular to this axis, fluid is being drawn in, i.e. to the sides. Pullers pull in fluid along the swimming direction, which is pushed away again perpendicular to that axis.

However, the force exerted by the flagella is not the only force exerted by the bacterium (Lauge and Powers, 2009; Yeomans, Pushkin, and Shum, 2014). Since bacteria are self-propelled particles living in an environment of low Reynolds number, all forces exerted on the fluid are counteracted by the high viscosity. In other words, no net force is applied by the bacterium. This means that the force exerted by the tail is counteracted by an equal and opposite force that is located at its head.

To describe the velocity field surrounding a single bacterium, the forces it exerts are added to the reduced Stokes equation (Lauge and Powers, 2009; Schwarz-Linek et al., 2016; Yeomans, Pushkin, and Shum, 2014). A lengthy derivation can be followed to simplify the velocity field into

$$\bar{v} = \frac{f}{8\pi\mu}\frac{l}{r^2}(3cos^2 - 1)\hat{r}, \tag{3.29}$$

in which f is the size of the force, μ the viscosity, r the distance from the bacterium and $\hat{r}$ the direction it faces.

Fluid and particles are dragged along the flow lines of the velocity field. The lines decay away from the bacterial force-dipole as $1/r^2$. Due to this decay, a non-spherical particle with finite size feels different velocities at its ends. This difference causes it to turn towards the flow line.

In other words, neighbouring bacteria are dragged along the flow field and reoriented by the $1/r^2$ decay in velocity (Lauge and Powers, 2009).

A second bacteria however shows similar behavior and movement, thereby producing a velocity field that has a similar effect on the first bacterium.

3.5 Bacterial collective motion

The interaction between bacteria grows increasingly complex for a larger amount of bacteria. To describe the hydrodynamic behaviour of a population of bacteria, a bacterial stress term is added to the Navier-Stokes equations (Koch and Subramanian,

2011). In short, it is given as

$$-\nabla p + \mu \nabla^2 \bar{u} + \sigma^B = 0, \tag{3.30}$$

in which σ^B is the bacterial stress term.

Above a critical concentration of bacteria, this stress results in spontaneously generated motion on scales larger than that of individual bacterial motion (Koch and Subramanian, 2011; Kasyap, Koch, and Wu, 2014a). Such motion has been reported to occur in the form of bacterial jets along the pinned contact line of an evaporating drop towards the center of the drop (Kasyap, Koch, and Wu, 2014b). The high concentration of bacteria required for this to occur is hypothesized to occur due to the evaporation-driven radially outward flow, explained in section 3.2.

However, to study the interaction of bacterial motion and evaporation-driven flow on the deposition pattern that forms, it needs to be investigated without the added complexity of this bacterial instability.

Before turning to the experimental methods, these few sentences briefly summarize the theoretical frameworks explained in this chapter.

The diffusion-driven evaporation of a sessile drop with pinned contact line has been discussed. The change caused by fluid leaving the drop is dissimilar to the change in drop shape due to the pinned contact line. This dissimilarity drives a radially outward flow towards the contact line, where colloidal particles deposit. Finally, the typical "run and tumble" movement of E.Coli bacteria has been discussed, in order to understand what effect on deposition formation this movement may have.

Chapter 4

Experimental methods

The goal of this research is to investigate how particle motility affects the deposition pattern in evaporating sessile drops with pinned contact line. To this end, several experimental requirements are described in this chapter. Data analysis methods will be discussed in the next chapter.

First, the setup will be discussed, in particular the requirements to observe the deposition pattern, drop shape and colloidal particle movement. Second, the E.Coli bacteria and accompanying experimental requirements will be elaborated upon.

4.1 Set-up

Two separate experiments are performed to make a sideview of the drop and a bottomview of the particles. In both, a $5\mu L$ sessile drop containing the fluorescent solutes is placed on a microscope cover slide.

A separate setup is used to obtain the sideview image. To measure the contact angle, the sideview is made to capture the drop shape. To this end, the drop is illuminated by a bar of light located 10cm behind the drop which shows a dark drop against a bright background. The contact angle can be measured manually or by the custom-made MATLAB script that determines the evolution of the contact angle over time.

To obtain images of the deposition pattern and to view the fluorescent particles, the setup shown in Figure 4.1 is used. As can be seen

The light omitted by a halogen lamp moves through a filter that passes only one wavelength. When this light illuminates the drop, its wavelength excites the fluorescent solutes. These solutes thereby emit light of a higher wavelength to fall through a microscope objective. Light of this wavelength is reflected by the filter. As such, only this light is captured by the CCD camera.

This setup has microscope objectives with a magnification factor of $2x$, $10x$ or $40x$. The camera is a Hamamatsu camera, with a maximum frame rate of $16f/s$ and a field-of-view (FOV) of 1344x1024 pixels. In the case of the $40x$ magnification, it views an area the size of $216.7\mu m$ by $165.1\mu m$.

PS-Fluored polystyrene colloidal particles that absorb a wavelength of $530nm$ and excite at $607nm$ are used as passive tracers. To track bacteria, green-fluorescent protein (GFP) will be used, which absorbs $475nm$ and excites $509nm$ [1].

[1] Though PS-Fluored particles are mono-disperse and should not cluster, but clustering has been observed. The presence of clustering colloids can be reduced partially before measurements or during post-processing. Before measurements, placing the container of particles inside the fridge or inside an insonification machine should remove clusters.

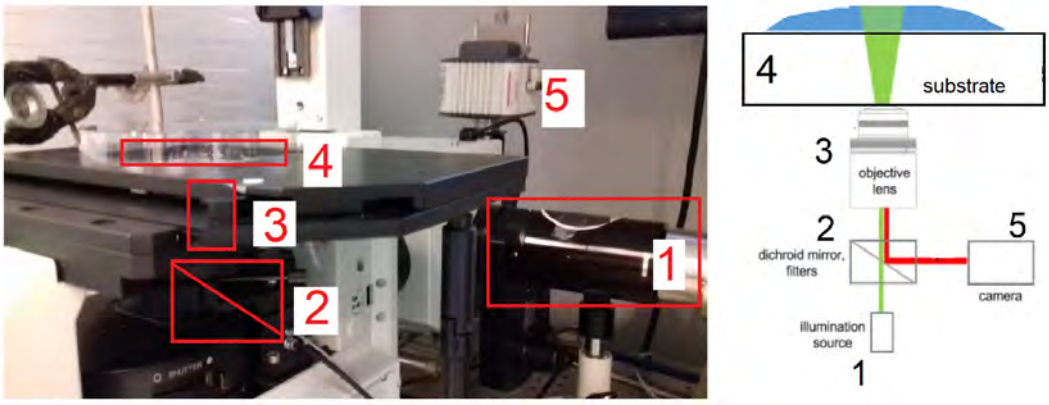

FIGURE 4.1: Picture of the setup used in this experiment (left) and schematic representation (right), showing halogen lamp as illumination source (1), dichroid mirror as GFP or RFP filter (2), objective lens (3), substrate glass (4), and camera (5).

A solution of colloidal particles is made by diluting 2.5%w/v (weight per volume) of PS-Fluored to a concentration of 0.01%w/v, corresponding to 10^14 particles/ml. The solution is made with distilled water or with a motility buffer, a nutrient-poor salt solution.

The motility buffer consists of $1.975gNaCl$ in $500mL$ water. This motility buffer is used for measurement on both passive tracers and on bacteria. Bacteria are grown, however, in a tryptone medium.

The tryptone medium in which bacteria grow consists of $10g/L$ peptone (made from caseine) and $5g/LNaCl$. These components are added to distilled water. The solution is subsequently disinfected in the autoclave, an industrial pressure chamber that raises temperature for a duration of time to sterilise the fluids placed within.

4.2 Culturing

In this research, two strains of E.Coli bacteria have been used. The first strain exhibits "run and tumble" movement as described in section 3.4. E. Coli have a typical propagation speed of $10\mu m/s$, a tumbling frequency of $1/s$, and a tumble time of $0.1s$.

The second strain has been altered via genetical modification to disable flagellar motion. In other words, this second strain does not propagate forward. Bacteria in this strain will be used as non-motile bacteria.

Further, other strains of genetically modified E.Coli do not fall within the scope of this research, but may prove of interest in future research. For example, a particular strain does not tumble but moves forward in a continuous run, whereas another strain does not run and only rotates.

The motile and non-motile E.ColiK12 strains are MG1655 with the genes POB335 and PTRC994.

Though colloids such as polystyrene particles may be left unattended for days or even weeks, populations of bacteria may not. Bacterial (propagating) behavior is

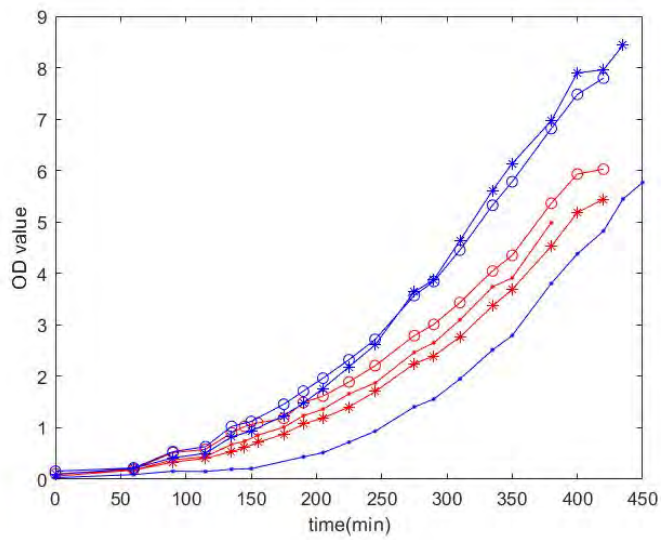

FIGURE 4.2: OD curve of motile (red) and non-motile (blue) E. Coli strains used in this experiment.

strongly dependent on their living conditions during experiments and during preparations. Evidently, additional care is necessary to enable reproducible measurements with bacteria.

To this end, a detailed protocol for measurements has been written. This protocol can be found in the Appendix. The remainder of this section will elaborate upon the growth of bacterial populations to clarify for which conditions the E.Coli bacteria show the highest motility.

The growth of bacteria populations depends on factors such as ambient temperature, pH-value, and presence of nutrients and oxygen, since these determine the reproduction rate. A single bacterium divides into two after consuming enough nutrients to grow to a certain size. In the correct environment, bacteria divide at such a rate that the population doubles exponentially over time. When nutrients, space or oxygen depletes, however, the growth rate decreases and the population may die. To prevent this from occurring, the population is transferred from the growth medium into a nutrient-poor motility buffer. In this buffer, bacteria can survive for a period of time but do not reproduce. This buffer is termed a 'motility' buffer, since bacteria portray high motility in search of nutrients.

To determine the concentration of bacteria, the optical density value (OD) can be obtained. The OD is a measure for the amount of biomass that has accumulated in the medium. Biomass constitutes of both living and dead bacteria, and as such grows exponentially with the bacterial growth curve and reaches a plateau when the population dies off. From the OD, the concentration can be approximated for estimation purposes by using an online tool, but needs to be validated by measuring a growth curve. The growth curve of bacteria constitutes of a lag phase, exponential phase, stationary phase and death phase. Bacteria are stored in the freezer. Upon arrival in the growth medium, bacteria adjust to the new environment. In this lag phase, the population does not yet grow. Once bacteria start dividing exponentially, the actively growing phase is reached. At this point, bacteria are transferred into the motility buffer.

The OD-plot of the motile and non-motile E.Coli strains used in this experiment

is shown in Figure 4.2. As can be seen, the plot does not yet level off. As such, it cannot be used to calibrate the OD value of measurements.

The OD of motile E.Coli strains of 7.608 in the measurement analyzed below corresponds to $6.0910^9 cells/mL$. The OD of non-motile E.Coli of 1.691 corresponds to $1.3510^9 cells/mL$.

Chapter 5

Data analysis software tools

The first section will first describe how particles appear in the particle tracking software. The second section describes the steps required to calculate velocities from these particle trajectories. The third section shows test data. The fourth section explains difficulties in detection and analysis.

5.1 General Defocused Particle Tracking (GDPT) analysis

General Defocused Particle Tracking (GDPT) is a MATLAB-based software package originally designed for particle tracking in three dimensions (Barnkob, Kahler, and Rossi, 2015).

GDPT measures the displacement of observed particles between successive frames of black-and-white images. This displacement is a measure of the instantaneous velocity of a particle at a certain point in time.

The particle observation by GDPT constructs data consisting of: coordinates (X and Y); displacement between successive frames (DX and DY); frame index (In) and index label of particle trajectory (ID). These data can be accessed in various ways, e.g. plotting the radial position as function of time or plotting the coordinates of a single trajectory at a time.

5.1.1 GDPT particle detection

The previous chapter briefly explained that the particles are observed by means of their fluorescence. The fluorescent signal emitted by bacteria or tracer particles passes through a wavelength filter and is subsequently captured by the camera.

In the images obtained by the camera, fluorescent particles are visible as bright circles with high contrast against a dark background. This contrast is a number between 0 and 255, for the 8-bit black-and-white images used here.

The contrast value can be used to locate particles. Particles of which the contrast exceeds a certain threshold are recognized. The threshold is one of several adjustable parameters in the software to fine-tune particle detection. Other parameters include minimum pixel area, maximum displacement value in four directions, and smoothing filters.

These filters can be used to remove Gaussian noise. The default filter settings are used in this research, i.e. $5x5$ kernel for Gauss filter and $3x3$ filter for median filter.

Objects in the camera view are observed as particles when their size and brightness value relative to the background mean both exceed the minimum value indicated by the parameter input. The effect of these parameters is illustrated in Figure 5.1. As can be seen, changing these parameters has an effect on which particles are detected. Panel (a) shows a default observation. Panel (b) has a higher threshold

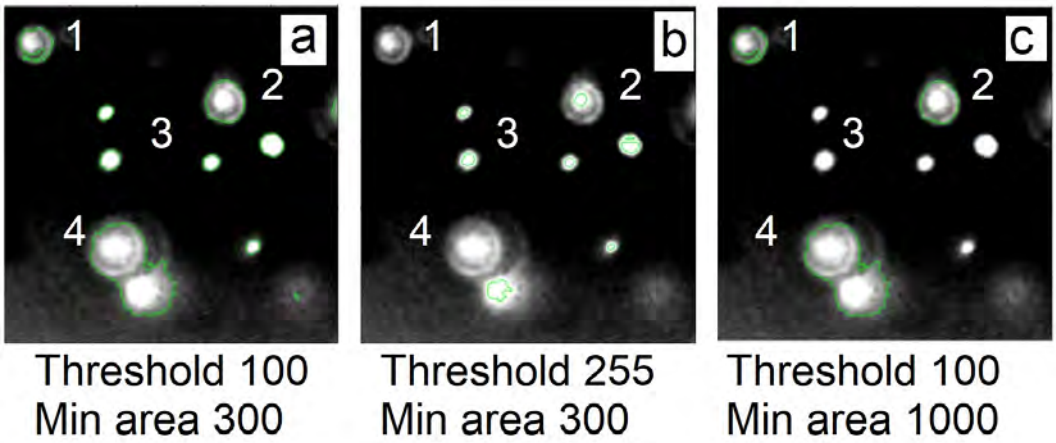

FIGURE 5.1: Image window showing the effect of changing the input parameters. Compared to panel (a), panel (b) shows only the brightest particles (3) due to a higher illumination threshold; whereas panel (c) shows only the largest particles (1,2,4) due to a higher minimum area.

and panel (c) has a bigger minimum area - while keeping the other parameters a constant.

Particle with an ID of (1) is observed in panel (a) but not in (b), because its brightness is higher than the threshold in (a) of 100 but lower than that of 255 in (b). Particle (2) has a bright center and diffuse outer ring. The ring is not observed at a higher threshold, but the bright center is. Particles surrounding (3) have an area smaller than the minimum area of 1000 pixels in panel (c) and as such are not observed. The slightly-out-of-view particles near (4) can be observed as a single particle in panels (a) and (c) or as two separate particles in panel (b), depending on the chosen parameters. This is due to the their diffuse edge.

In "Tracking mode", particle trajectories are made by comparing the positions of particles in subsequent images. At a certain particle ID's location (X, Y) at frame In, an observation window is defined. If a particle is found in this window at the next frame $In + 1$, the particle is given the same ID. The difference in location between these two particles constitutes the pixel displacement numbers DX and DY. Once a trajectory exceeds a few particles in length, the software narrows its search window in the following frame to match the expected path of the trajectory (**barnkob2015**).

A particle's location at a next frame may fall outside of the observation window, due to large displacement. If the window does not encompass the new location, it will not be detected and the trajectory ends. Then, the window has been too small.

Conversely, if another (new) particle appears it the window, it may be detected as being part of the trajectory. Then, the window has been too big.

In other words, the observation window size is an important parameter in observing particle displacement correctly. It is determined by $\Delta xmin, \Delta xmax, \Delta xmin$ and $\Delta ymax$, which sets the maximum displacement in all four directions.

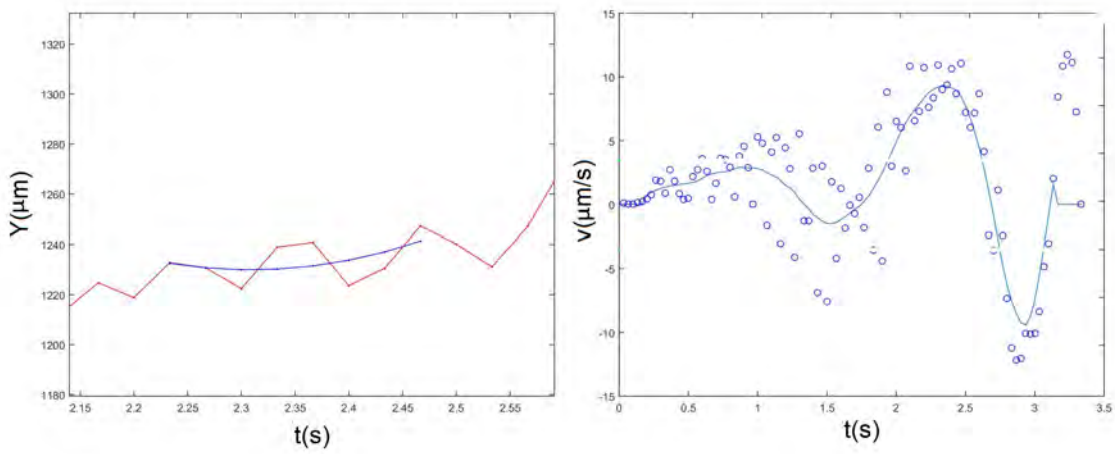

FIGURE 5.2: Y-position of a test particle observed in GDPT plotted as a function of time showing oscillations (red, left) and a parabole fitted through a selection of points (blue, left) from which the velocity is calculated. The selection of points moves over the trajectory to determine the velocity at each point in the particle trajectory. As such, original velocity data in the right panel (blue circles) are smoothed (blue curve).

5.2 Data analysis

Y-position of a test particle observed in GDPT plotted as a function of time showing oscillations (red, left and middle) and a parabole fitted through a selection of points (blue, left) from which the velocity is calculated. The selection of points moves over the trajectory (middle) to determine the velocity at each point. As such, original velocity data (blue circles) are smoothed (blue curve)

The first and last points of the trajectory are not considered, since these do not have a sufficient amount of neighbours. Because of this, the window size has an upper limit above which too many data points or short trajectories are discarded. A second upper limit is determined by the size of fluctuations in data that are to be considered. The window is required to encompass the small-scale oscillations it filters, but not the larger motions. In the case of these experiments, a minimal window size is 4, a maximum 7.

5.3 Test data validation

To validate the GDPT software and input parameters, tests data are generated. Test data constitute of a series of images containing (virtual) particles of which the position and displacement determined manually. [1]

Test data generation starts with an image of strings, displayed in panel (a) of Figure 5.3 on the left. Each string is turned into data points (x, y, t) describing a particle moving along the path determined by the string. At each time t an image is generated containing particles at the positions (x, y). This series of images is analyzed in GDPT of which the results are compared to the predetermined strings. The GDPT data are displayed as trajectories in panel (b) of Figure 5.3 on the right. As can be seen, the trajectories correspond to the actual strings.

[1] These have been generated by Ad Holten, whose work is appreciated greatly.

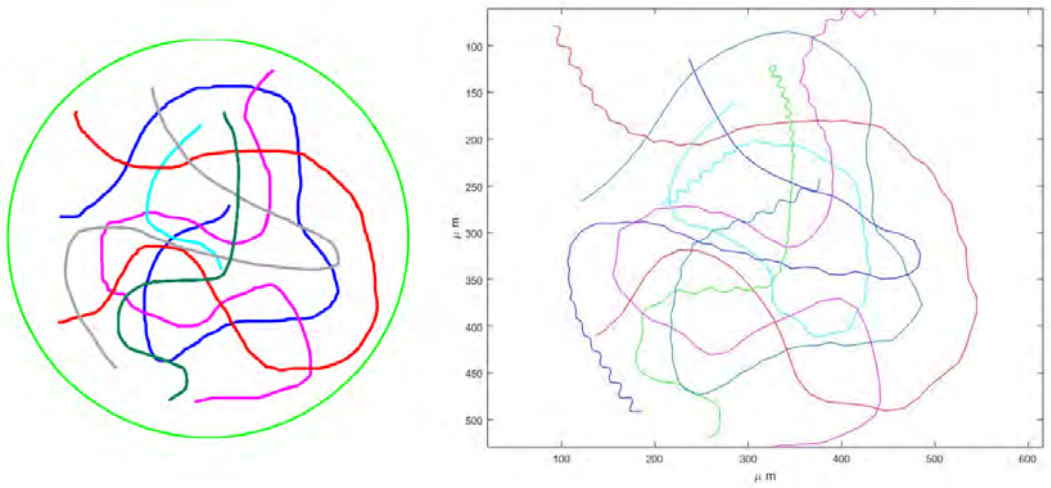

FIGURE 5.3: Strings from which test data is generated (left), which has been analyzed in GDPT and displayed as trajectories (right). In data generation, a sine is added to the strings, which is observed with GDPT but not shown in the original strings.

To determine the accuracy of GDPT, in particular to small-scale oscillations, a sine is superposed into the test strings. This oscillation may be compared to random Brownian motion or other small-scale motion of a particle as it moves along a certain path. As can be seen from Figure 5.3, these oscillations can be observed without showing errors.

Additionally, it shows how data respond to a filter that may be applied to remove small-scale motion. The filter used in this research is a parabolic fit that moves along each trajectory to determine the velocity at each point, which is displayed in Figure 5.2.

5.3.1 Erronous particle detection

The software may also observe a number of irregularities resulting in erroneous particle detections, such as clusters of particles; particles too close to each other; particles out of focus; other optical irregularities; and erronuous input parameters. Conversely, particles may miss detection due to several reasons, such as low particle illumination, high background light, or a diffuse particle edge. These various irregularities will be discussed below.

A first irregularity is clustering of particles. Though the fluorescent particles are monodisperse and bacteria should not cluster, clusters of particles may appear. Clusters generally appear as larger, irregular patterns. These patterns decrease accuracy of measurements in two ways. First, a cluster does not function as tracer for the ambient velocity due to its size and inertia. A cluster may move slower than the mean flow. Second, the badly defined edges of a cluster may lead to irregular jumps. In other words, when the edges of the cluster shift, it may appear as if the observed particle has been displaced.

Clusters can be partially prevented by finetuning the appropriate settings and threshold in GDPT or by post-processing outlier removal, which will be discussed in the final section of this chapter.

When particles move too close to each other or even collide, particle detection may mistakenly observe these particles as a single particle. An example of this is particle (4) in Figure 5.1. This is due to the minimum area required to observe the nonzero size of particles. A particle is detected, because it has an area with brightness higher than the background. However, when a second particle is too close, there is an overlap of the particles.

This depends on brightness profile, contrast, threshold value, and the minimum area for identifying particles. Before and after collision, the software may identify the constituent particles separately.

The particle tracking software may identify colliding particles separately before and after collision, but as a single particle during collision. Due to this difference or due to this gap, the software may interchange the colliding particles when ascribing trajectories.

Though it is assumed that the vertical flow velocity is relatively small [2], particles may move in the vertical direction and thereby move in or out of focus.

The depth of focus in this setup is several particle sizes big. As such, particles may be in view but out of focus.

Particles out of focus appear diffuse, due to an apparent increase in size but decrease in brightness and contrast. As it turns out, particles (1), (2) and (4) in Figure 5.1 are out of focus. Their edges are less sharp than particles in focus. Instead the bright center blurs into the dark background. These diffuse particles may miss GDPT detection and instead form a background illumination that hinders particle detection, similar to what has been discussed for particles too close to each other.

5.4 Outlier removal

Outliers may be prevented by the correct use of parameters in GDPT. However, these parameters cannot be perfectly adapter to imperfect data. As such, some outliers remain that need to be deleted by post-processing steps. These steps include detection and removal of outliers, as will be elaborated upon below.

Outliers in the data occur in the form of displacements that do not coincide with actual particle movement. For example, Figure 5.5 shows an incorrect jump in a particle trajectory produced by GDPT.

Figure 5.5 shows a particle trajectory produced by GDPT. As can be seen, an outlier in the trajectory occurs in the form of a displacement that does not coincide with the actual movement of a particle. This typically occurs when a neighbouring particle is mistaken for the particle that is being currently followed, or when the initial particle moves out of view.

To detect outliers, a simple threshold value above which a displacement is incorrect does not suffice. This is because there may be incorrect displacements that are smaller than actual movement of particles. This occurs when the distance between neighbouring particles is smaller than the displacements.

The displacement of bacteria and the displacement of colloids Instead of a simple threshold, a relative threshold is opted for. If, relative to the median displacement of a trajectory, a displacement exceeds a threshold factor, it is viewed as outlier.

[2] Due to the small vertical velocity of the flow, the 'defocused' functions of GDPT to track particles in three dimensions are not considered in this research.

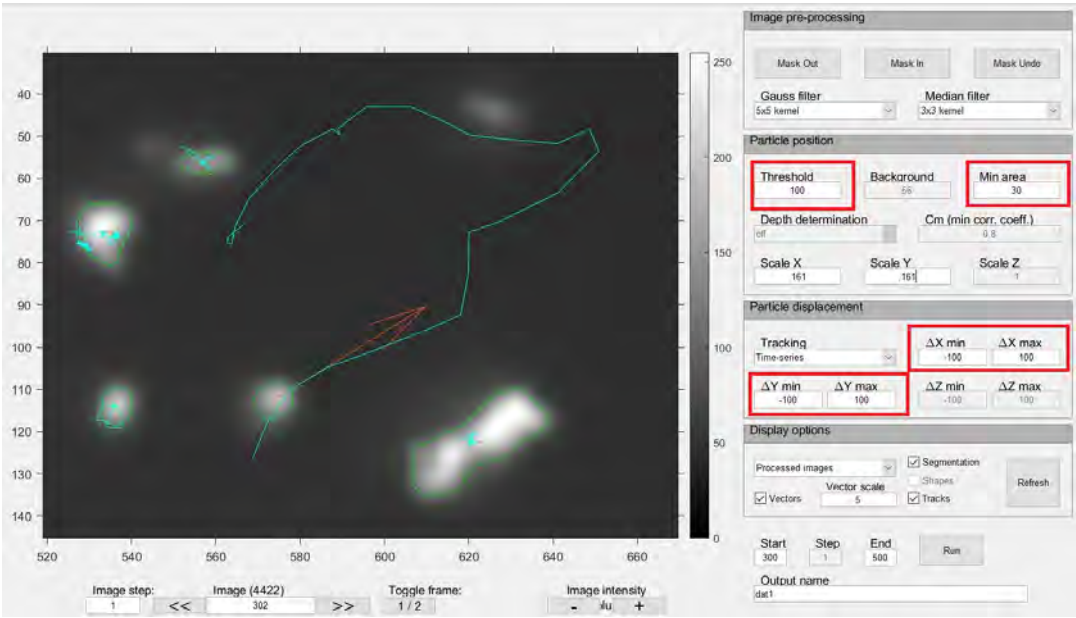

FIGURE 5.4: Camera view of fluorescent particles with 40x magnification objective analyzed with General Defocused Particle Tracking (GDPT) software. The legend on the right in the top image shows the brightness values, ranging from 0 to 255, corresponding to the 8-bit black-and-white images. Particles sufficiently bright against the dark background are detected and encircled (green). Lines indicate the trajectory of particles over time (green) and arrows indicate the instantaneous displacement of the particle between the current frame and the next frame (orange). The red boxes in the bottom image show the adjustable paramters to fine-tune detection: the illumination or contrast threshold; the minimum pixel area; and the maximum displacement.

These outliers are removed by deleting the incorrect displacement, thereby effectively cutting the trajectory into two. This is done by assigning a new ID value to the second half of the trajectory, as can be seen in Figure 5.5.

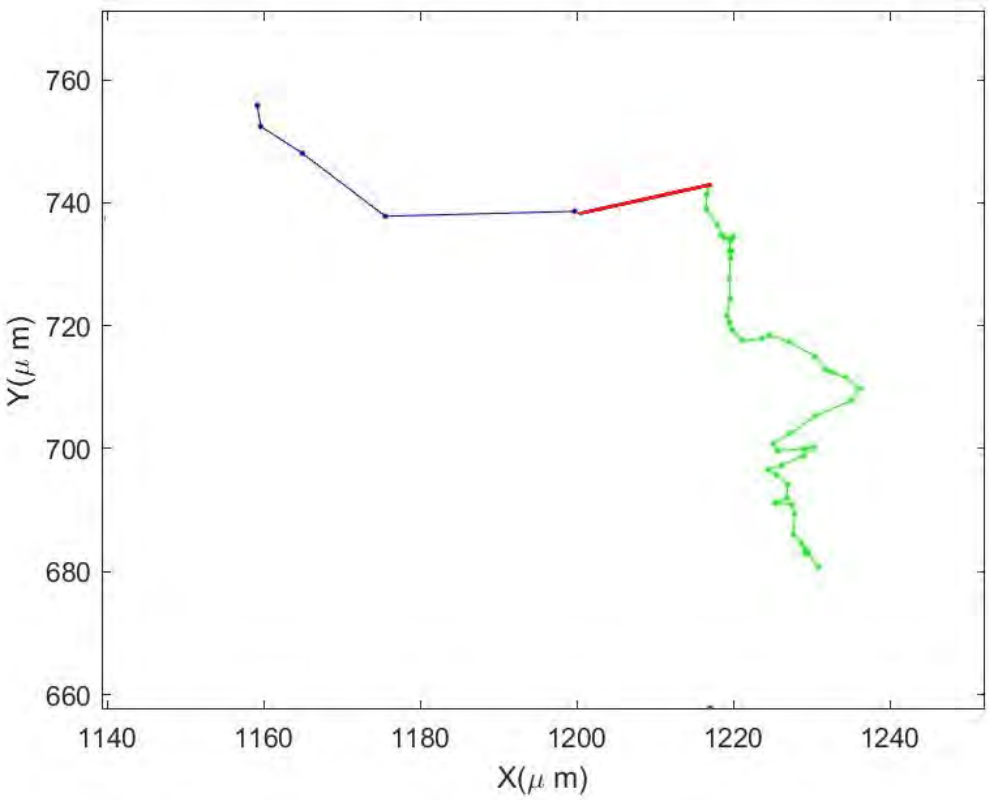

FIGURE 5.5: GDPT detection of particle trajectory processed with outlier detection, showing the full trajectory in all three colors, split into first trajectory (green), incorrect step (red) and new trajectory (blue).

Chapter 6

Results

This chapter reports the findings of the experiments. The first section describes the deposition pattern and velocity measurements of the GDPT measurements. We used a drop of water containing passive colloids as a test measurement, in order to compare the following measurements. The second section describes the changes in the pattern and flow profile resulting from using buffer as experimental drop. The final section describes various findings on drops of motile and non-motile bacteria in buffer solution in an attempt to answer the research question posed in chapter 3: how do self-propagating E.Coli bacteria deposit in an evaporating drop and can this compared to the deposition of passive tracers?

6.1 Passive colloids in water drop

When a drop of water containing colloidal particles evaporates, it leaves a ring-shaped stain (Deegan et al., 1997b). Figure 6.1 shows the deposition pattern of a drop of distilled water containing fluorescent colloidal particles.

The $1\mu m$-sized particles in the solution had a concentration of 0.1% weight percent in a $5\mu L$-sized drop. The images were obtained with the fluorescent signal emitted by the colloids at magnification factor of $40x$ in panel (a) and $2x$ in panels (b) and (c). As can be seen, the colloids concentrate in a ring-shaped stain.

Panel (a) shows that the ring-shaped stain is visible as bright outer ring around a darker inside region. The top half of the contact line has depinned, resulting in an additional ring with deposited particles, shown in panel (b).

Panel (c) shows an ordered pattern of particles below the red line and disordered packing above it. This transition from order to disorder indicates that the rush hour phenomenon has occurred. This observation displays the behavior that has been reported in previous research (Marin et al., 2011).

The contact line of a water drop has been observed to depin in multiple experiments. This can partly be attributed to the substrate used in the experiment.

The $40x$ objective has a working distance of $0.51mm$, which is smaller than the typical substrate glass. Instead, a microscope cover slide is used, which is sufficiently thin to fit within the objective working distance. A necessary trade-off accompanying these cover slides is its lower surface roughness. These cover slides appear to be relatively smooth for pinning. Pinning is most likely to occur on a rough substrate, by irregularities on the substrate, or by solute deposition near the contact line which is known as 'self-pinning'. As such, drops of distilled water may show little pinning on the cover slides.

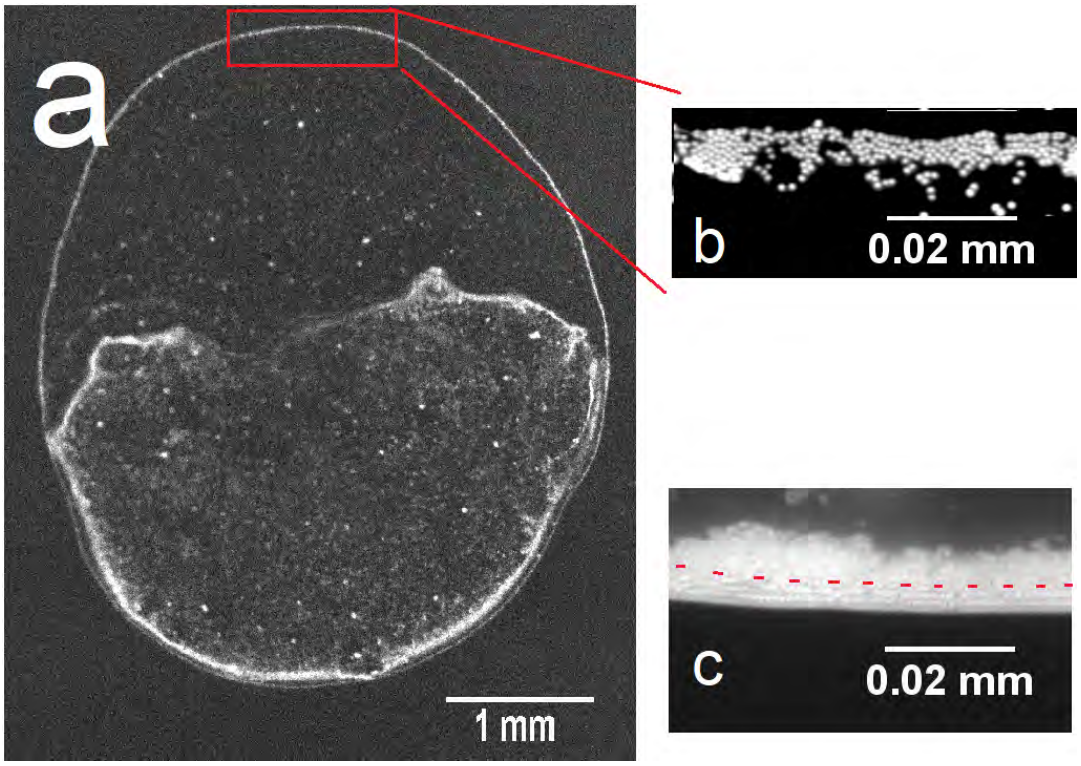

FIGURE 6.1: Deposition pattern of a water drop containing fluorescent colloidal particles viewed with $2x$ magnification in panel (a) and $40x$ magnification in panels (b) and (c). Panel (b) is a close-up of (a), showing the stain before depinning. Panel (c) shows an ordered pattern below the red dotted line and a disordered phase above it.

In the experiment to measure the velocity of passive tracers in the water drop, the configuration was as follows. In following experiments, on buffer or bacteria, the same configurations were used, unless specified otherwise.

The camera settings had a framerate of $4fps$ and exposure time of $30ms$. With this exposure time, the high concentration of colloids in the contact line resulted in an overexposed signal. The contact line was removed by cropping the images during GDPT analysis. This reduced the camera's FOV of $216.7x165.1\mu m$ to $216.7x100\mu m$. As such, data were taken at radial position $R - r$ in the region of $[65.1; 165.1]\mu m$.

The $5\mu L$-sized drop has an initial contact angle of $45°$ and base radius of $3mm$.

The $1\mu m$-sized particles in the solution had a concentration of $0.01\% w/v$, weight per volume. Evaporation time was $550s$ and the humidity 27%.

The velocity of passive tracers in the drop of water as observed with GDPT is displayed in panel (a) of Figure 6.2. As can be seen, the radial velocity increases over time in accordance with the theoretically expected capillary flow, Equation 3.24 indicated by the black line. In contrast, the velocity in the tangential direction does not exceed the magnitude of random Brownian motion, which is calculated with Equation 3.28 and time t of $0.25s$ between frames to be $v_b = 5\mu m/s$.

Typical particle trajectories in this measurements as observed by GDPT are displayed in panels (b) and (c) of Figure 6.2. Plotted in each graphs are the trajectories of particles that are observed at frame 620 (b), before the increase in velocity, and frame 2080 (c), after the increase.

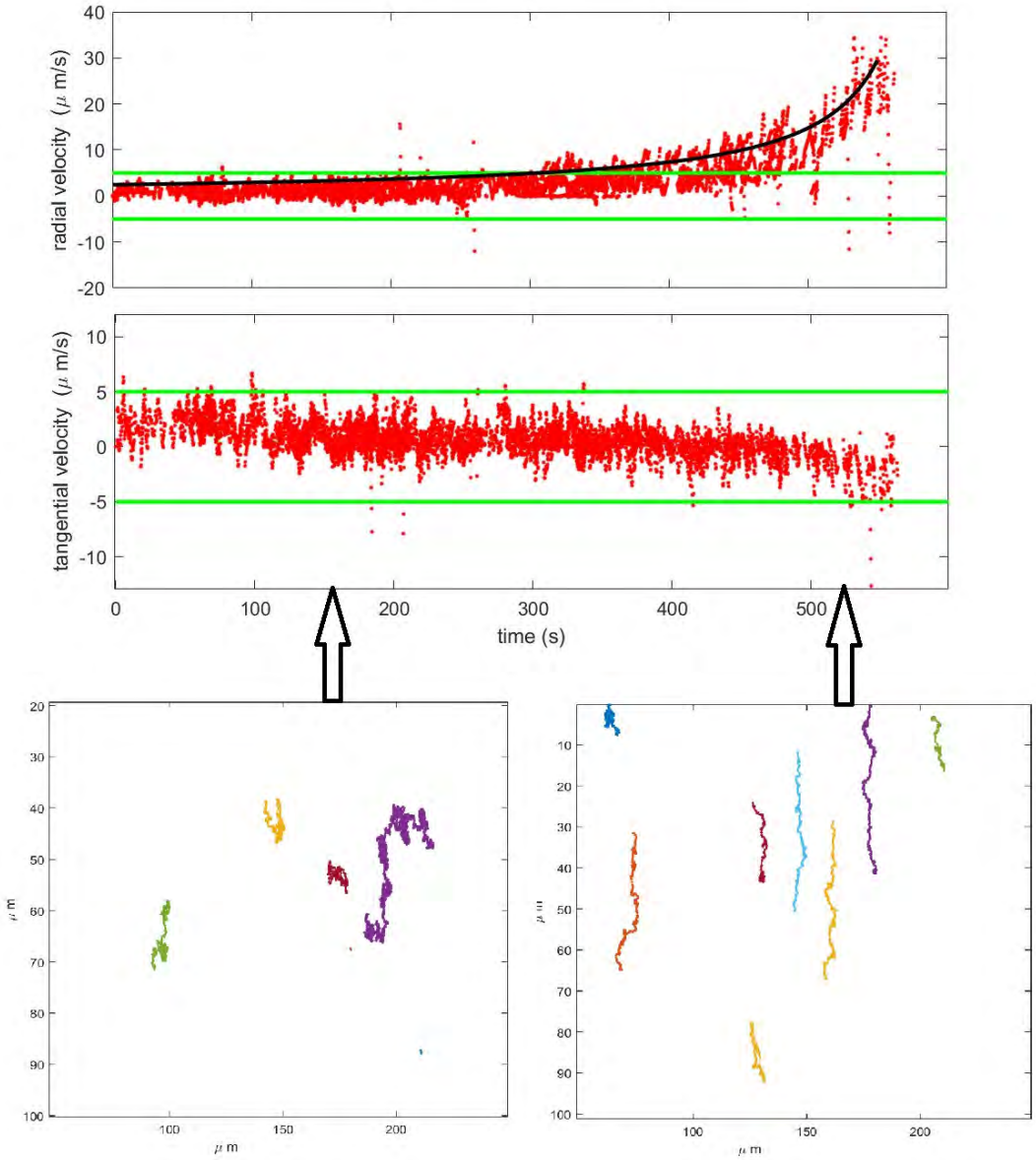

FIGURE 6.2: Radially outward velocity (top) and tangential velocity (middle) of passive tracers in drop of water as measured with GDPT (red). The solid black line corresponds to the theoretically expected capillary flow, Equation 3.24. The green solid lines correspond to the magnitude of random Brownian motion, Equation 3.28. The $5\mu L$-sized drop has an initial contact angle of $45°$, base radius of $3mm$; and the humidity is 27%. Panels (b) and (c) show the particle trajectories observed by GDPT at a time of $160s$ (left) and $520s$ (right). Panel (b) shows random motion with a magnitude of $3\mu m/s$. Panel (c) shows movement towards the contact line below with a magnitude of $20\mu m/s$.

As can be seen, panel (b) shows movement in all directions with a magnitude of $3\mu m/s$ whereas panel (c) shows predominantly movement towards the contact line with velocities in the order of $20\mu m/s$.

From Figure 6.2 it appears that particles move randomly early in drop evaporation, but follow the high radially outward velocity at later times. Considering the framework established by (Marin et al., 2011), this increase in flow towards the contact line explains the deposition pattern shown in Figure 6.1, in particular the transition from ordered to disordered packing.

6.2 Passive tracers in motility buffer drop

The following section describes the measurements on passive tracers in a drop of motility buffer solution. Measurements were performed on a $5\mu L$-sized drop with a concentration of $0.1\% w/v$ $1\mu m$-sized colloidal particles.

The deposition pattern is shown in panels (e-h) in Figure 6.3.

Panels (f) and (h) are made with RFP illumination showing only the fluorescent signal emitted by the colloidal particles. As can be seen, the colloids concentrate in a ring-shaped stain. In panel (g), the particles are slightly out of focus and overexposed, making it difficult to discern individual particles. Panels (e) and (g) are made with brightfield illumination, showing salt crystals. These crystals are not visible in the fluorescent image.

In the fluorescent image, light with a wavelength of $530nm$ illuminates the substrate, but a wavelength of $607nm$ enters the camera, due to the wavelength filter. The fluorescent colloids are observed because they absorb $530nm$ and emit $607nm$. Salt crystals, however, reflect the light of $530nm$, which is blocked by the filter and is not captured by the camera. The salt crystal appears to be present over the entire stain, whereas the solutes deposit only in the contact line.

In the experiments, two distinct deposition patterns have been observed to form, as shown in panels (a) and (b) of Figure 6.4. As can be seen, a disordered contact line deposition and a homogeneous deposition occur.

These observations have been made in measurements with identical configurations but performed on different days. As such, droplet size and concentration were identical, but humidity, substrate cleanliness and other less controllable parameters may have varied. For example, observed humidity values range between 20% and 35%.

Both observations will are discussed separately in sections 6.2.1 and 6.2.2 respectively.

6.2.1 Disordered pattern

The disordered contact line deposition in panel (a) of Figure 6.4 shows the formation of small structures, indicated by red boxes.

This is dissimilar to the disordered patterns observed in previous papers and in section 6.1. The previous patterns showed smaller spacing between particles (Marin et al., 2011). In other words, the packing of these buffer deposition patterns is smaller when compared to previous findings which have been attributed to the rush-hour phenomenon

To inspect the pattern formation of this drop in more detail, the particle trajectories during the end of evaporation and velocity plots are investigated. These are

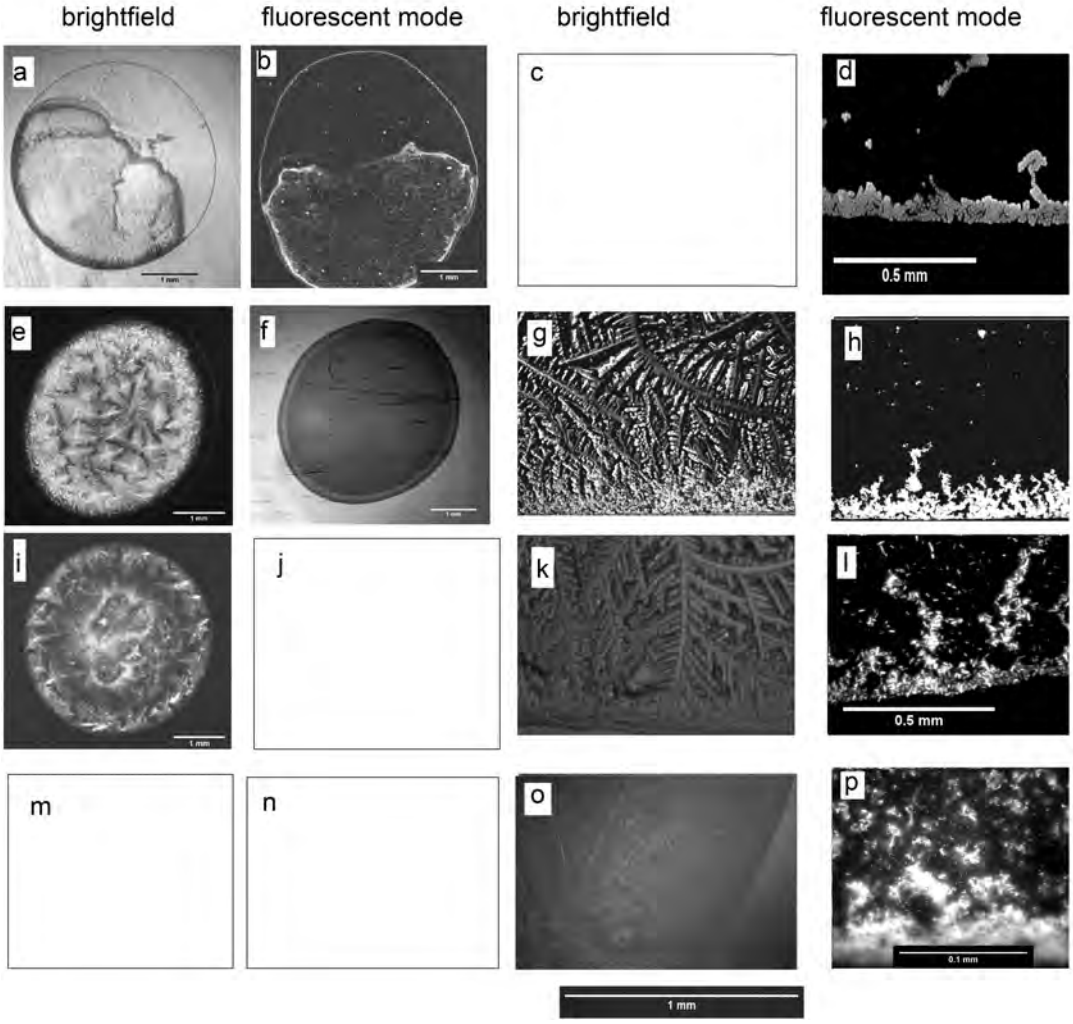

FIGURE 6.3: Deposition patterns of fluorescent colloidal particles in drop of water (a-d) or motility buffer solution (e-h) and of motile (i-l) and non-motile (o,p) E.Coli strain in motility buffer. First and third columns are viewed with brightfield; second and fourth in fluorescent mode, i.e. RFP for colloids and GFP for bacteria. Third and fourth column are close-up views of the first and second column. Concentration of colloids is $0.01\%w/v$; motile E.Coli $6.09 * 10^9 cells/ml$; non-motile E.Coli. Scale bars are $1mm$, unless indicated otherwise; panel (p) is $0.1mm$.

shown in panel (c) and (e) of Figure 6.4, respectively. As can be seen, these show no significant deviation from the observations of the water drop discussed in section 6.1.

Instead, the disordered contact line may be caused by the clustering of the colloidal particles. When viewing the growth of the contact line in subsequent images, it can be seen that the structure follows directly from the clustered particles that enter the contact line.

The fluorescent particles used in this study are monodisperse, i.e. non-clustering, due to a small positive charge that repels other particles. It is hypothesized that the presence of salt ions affects this repellent interaction, increasing the probability of clustering.

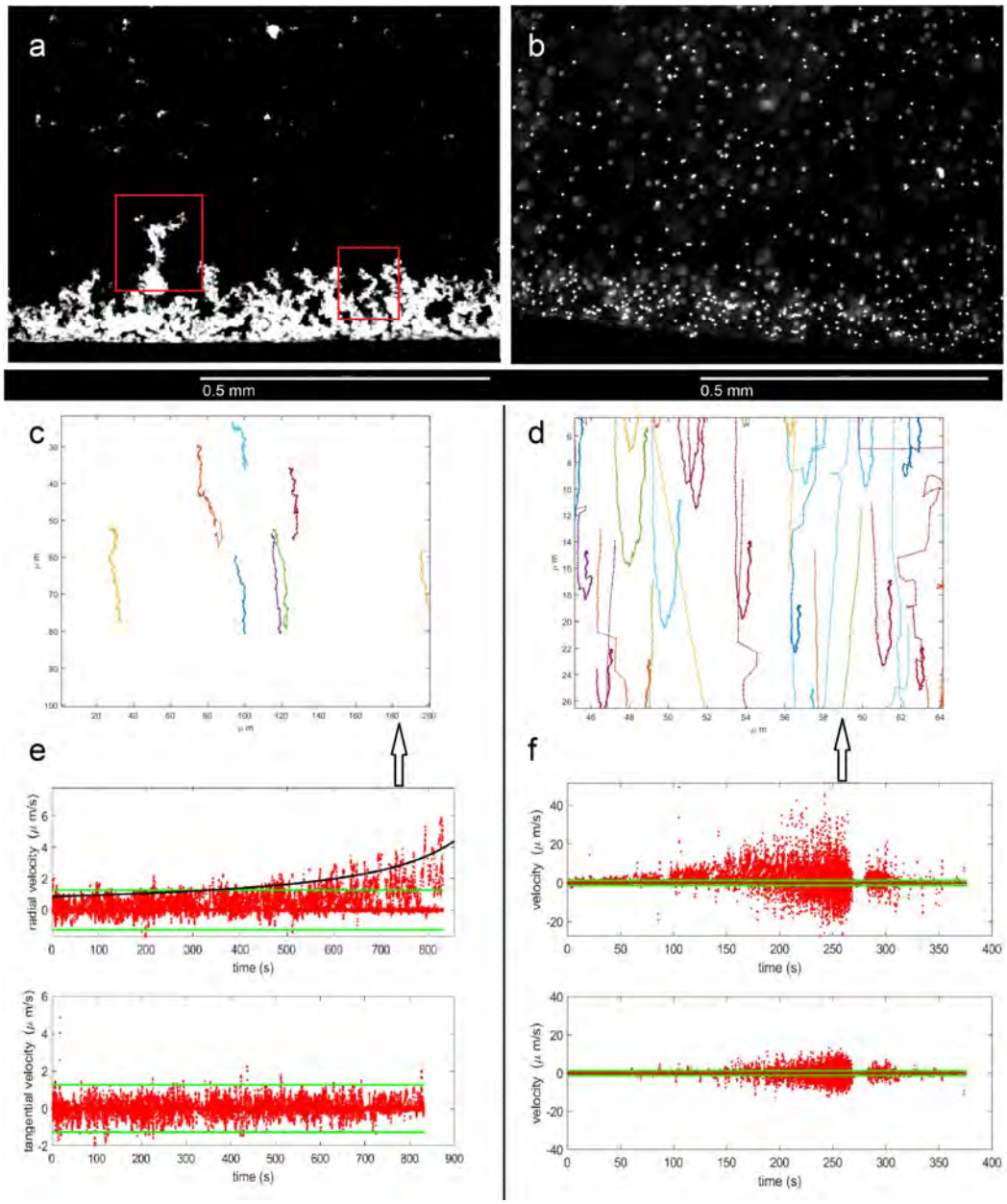

FIGURE 6.4: Two different deposition patterns of a motility buffer drop under 10x magnification (a,b), showing particles disorderedly concentrated in the contact line (a) and shows a homogeneous distribution of particles (b). Typical particle trajectories (c,d) indicate movement towards the contact line (c,d) but also a turn into the opposite direction (d). Radial and tangential velocity plotted over time (e,f), showing GDPT measurement in red, theoretically expected capillary flow in black and magnitude of random Brownian motion in green.

6.2.2 Homogeneous deposition of passive colloids in buffer drop

The homogeneous deposition resembles the pattern corresponding to that of a drop with receding contact line, which also shows a uniform pattern (Parsa, Harmand, and Sefiane, 2018). However, the contact line has remained pinned. A receding contact line is not expected to occur for a self-pinning drop such as the drop of buffer.

Evidently, it is necessary to inspect the motility buffer drop more closely. [1] As before with the drop of water, the colloids are used as passive tracers to map the flow velocity.

To understand the homogeneous pattern, its development over time is inspected using the velocity plots, particle trajectories, and the raw image material.

The velocity plot in panel (f) of Figure 6.4 indicates several irregularities. The velocity towards the contact line (the positive radial velocity) increases over time. However, it also increases in the opposite direction. As can be seen from the particle trajectories, some particles move towards the contact line which is located below the image, but are dragged in the opposite direction before reaching it. This occurs after $t = 180s$, which is before half the evaporation time of $400s$.

Figure 6.5 hints to a vertical component in particle movement. The top image shows particle movement towards the contact line below at half the evaporation time. The bottom images show, over subsequent frames located at one region in the green band, a particle moving into focus. Recall from section 5.3.1 that particles out of focus appear different from particles in focus. In other words, particles out of focus appear larger and diffuse (Barnkob, Kahler, and Rossi, 2015).

At $170\mu m$ distance from the contact line, indicated by the green band, few particles move between $200s$ and $250s$. This indicates a band of zero horizontal velocity, or a stagnant point. Instead, particles move in from a different height.

At approximately $100\mu m$ from the contact line between $200s$ and $250s$, particles oscillate in both the radial direction and the vertical direction. Finally, the entire velocity field approaches zero at $t = 260s$, due to particles and the contact line moving out of view. The final section of nonzero velocity corresponds to the re-entry of particles into the FOV before settling in place.

These phenomena, i.e. the stagnant point and vertical movement, indicate the presence of Marangoni circulation as the result of salt concentration gradient across the drop, which will be explained shortly. A sketch of the hypothesized Marangoni flow is given in the bottom image of Figure 6.5.

The nonzero concentration of salt in the drop increases when water leaves during evaporation. Since evaporation is non-uniform across the drop radius, the salt concentration increases nonuniformly during evaporation. Therefore, the concentration increases most near the contact line. Surface tension scales with the salt concentration and acquires a similar gradient towards the contact line. Fluid flow thereby arises near the region of high surface tension (Rapp, 2016).

The evaporation time of the drop with homogeneous pattern is half that of the drop with disordered contact line. This quicker evaporation may have shown itself in higher temperature gradients that lead to surface tension gradients. As such, temperature-induced Marangoni flows may have formed, explaining the additional flow (Still, Yunker, and Yodh, 2012).

However, this flow does not occur if the surface tension gradient is repressed. For example by the presence of surfactants that lower surface tension. In other words, the presence of dust particles may prevent Marangoni circulation from occurring.

[1] A sideview image of a drop can indicate when the contact line recedes. However, measurements in this experiment have been performed on a setup without a sideview camera.

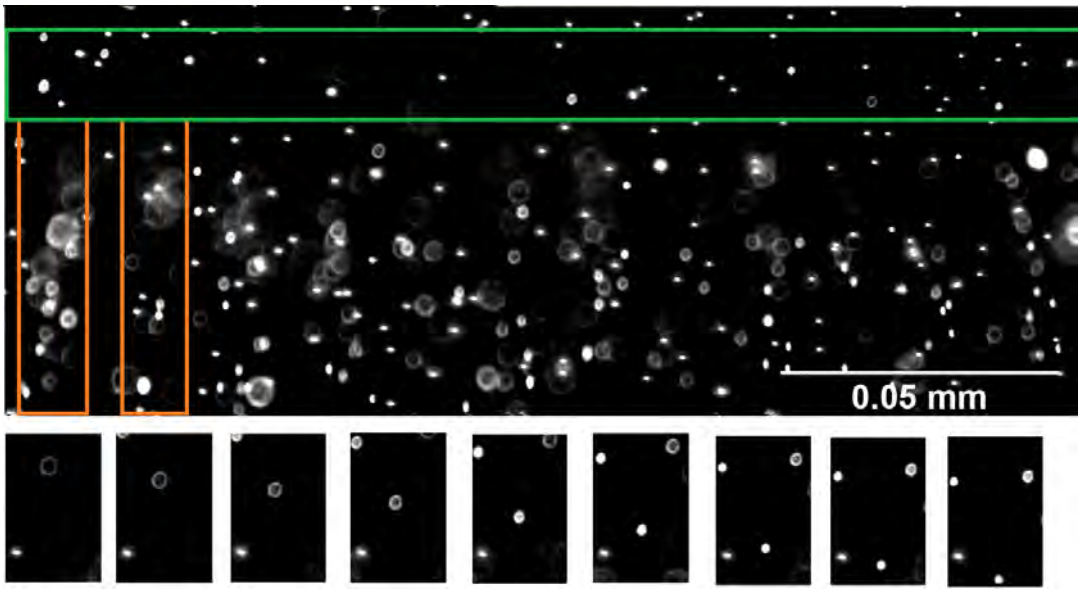

FIGURE 6.5: Snapshot of evaporating motility buffer drop with passive tracers at half the evaporation time with contact line below the image. Green lines in top image indicate a stagnant band with nearly zero horizontal velocity. Orange lines show that particles move in bands towards the contact line, between which little movement is observed. The figures in the middle show evolution over time of a small region, showing a typical particle that moves in focus before moving toward the contact line, indicating vertical movement. The bottom figure shows a sketch of a vortex and stagnation point that may have arisen.

6.3 Motile E.Coli bacteria

The deposition pattern of motile E.Coli is displayed in panels (i), (k) and (l) of Figure 6.3. Panel (i) shows the entire stain with $2x$ magnification and panel (k) with $10x$ magnification, both in brightfield illumination. Panel (l) shows $40x$ magnification in fluorescent mode. From this pattern, two observations can be made. As can be seen, the contact line shows a number of clustering structures growing out of the contact line. In these structures, bacteria are oriented seemingly random. In contrast to this, a small region at the outer perimeter of the contact line shows bacteria that appear more ordered. These bacteria are aligned parallel to a few neighboring bacteria.

The movement of E. Coli has been discussed in more detail in Chapter 3. E. Coli propagation speed typically is $10\mu m/s$ during run events. Tumbles occur with a frequency of $1/s$, and a tumble time of $0.1s$.

Figure 6.6 shows a typical GDPT observation of motile E.Coli bacteria. As can be seen, particle trajectories may change direction in various ways.

In the orange box, the particle trajectory shows a gradual change in orientation. As discussed in section 3.4, E.Coli do not move in a straight line due to rotary diffusion.

In the green and red boxes, particle trajectories show a sharp turn. Such turns can be caused by either a tumble or by an incorrect observation. These two causes may resemble each other but show differences. Both involve the detection of a particle

at a random angle from the initial trajectory. The main difference between tumble and incorrect jump is the magnitude of the displacement relative to the initial trajectory, which is bigger for the incorrect jump. As can be seen in the red boxes, the particular change in direction entails a large displacement when compared to the rest of the trajectory. On the other hand, the two turns observed in the green box, corresponding to a tumble, show no such jump.

This relatively large displacement is incorporated into the outlier detection in order to remove the incorrect jumps, as has been discussed in Chapter 5.

Further, the blue box indicates an observed particle that shows little movement. This corresponds to an immobilized bacterium. Such a bacteria may be dead or stuck to the substrate.

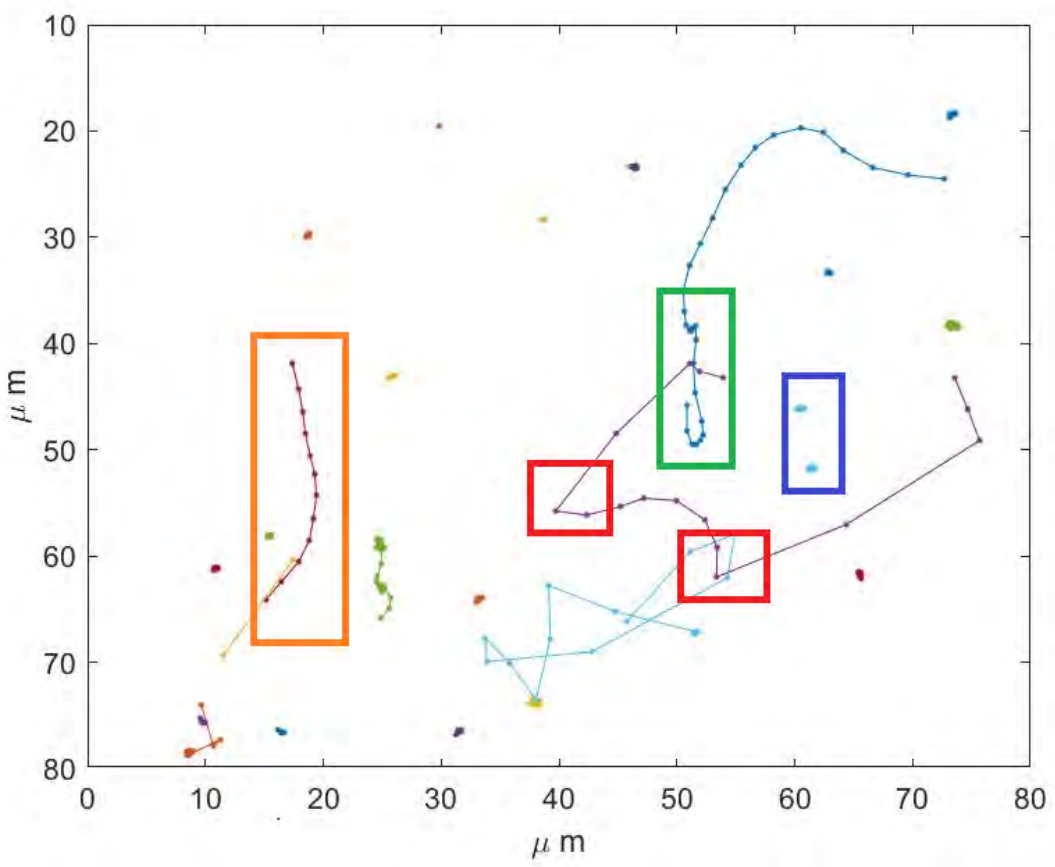

FIGURE 6.6: GDPT observation of a number of bacteria trajectories, showing rotary diffusion (orange), tumble (green), incorrect jump (red), and immobile bacterium (blue).

The velocity of motile E.Coli strain in motility buffer solution as observed with GDPT is displayed in panel (a) of Figure 6.7. In this particular measurement, the evaporation time is 1600s. The OD value of 7.608 corresponds to $6.09 * 10^9$ cells/ml.

As can be seen, the radial and tangential velocity decreases in the time period between

After 1200s, the positive radial velocity increases. In contrast, the velocity in the tangential direction and the negative radial velocity do not exceed the magnitude of random Brownian motion.

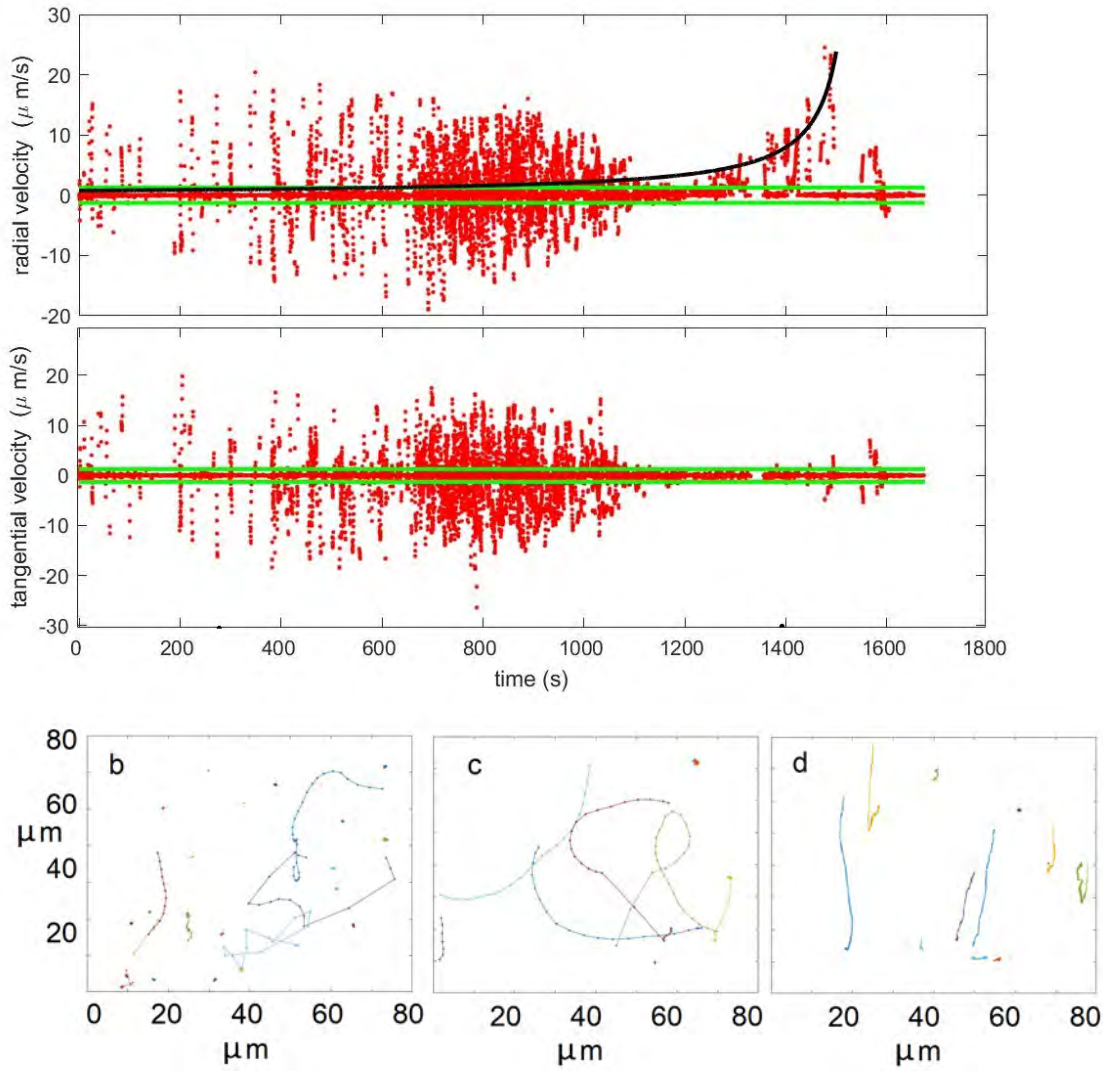

FIGURE 6.7: GDPT analysis of motile E.Coli strain in $5\mu L$ drop of motility buffer solution with concentration of $6.09 * 10^9$ cells/mL Panel (a) shows velocity (red) in the radial direction (top) and tangential direction (bottom) after GDPT processing and outlier removal, plotted as a function of time. The black curve corresponds to Equation 3.24. The green lines indicate the magnitude of random Brownian motion, Equation 3.28. Panels (b), (c) and (d) show trajectories observed at a time of 200s (b), 800s (c) and 1500s (d) of motile bacteria in a drop with total evaporation time of 1600s.

Many data points show a zero velocity, indicating no movement. These are the result of immobilized bacteria, as has been shown in the blue box in Figure 6.6.

The region of time $0 < t < 700s$ shows fewer data points than later in the measurement. This must be a result of GDPT observations, since the amount of bacteria does not increase in this period of time. In other words, a smaller amount of bacteria is observed by GDPT in the first 700 seconds. As discussed in section REF, this may have several causes.

The displacement of bacteria between frames may be too high to be discerned, either for the observation window used in analysis or due to the amount of bacteria. Additionally, bacteria may appear unclear when compared to other bacteria and

the background image. The presence of immobilized bacteria dispersed over the FOV as mentioned in Figure 6.6 may point to difficulties in GDPT analysis. When a swimming bacterium passes by an immobilized bacterium, it may not be observed for one or several frames.

This difficulty is no longer a problem when the immobilized particles are no longer visible in the image. As explained in Figure 6.6, the immobilized bacteria fade out of view over time. As such, GDPT observes more bacteria after $700s$, thereby showing more data points in Figure REF.

These observations of bacterial motility changing over time can be used to gain insight into the observed deposition pattern. First, a small reminder of how passive colloids form a deposition pattern.

Colloids are dragged towards the contact line and fluctuate in place due to Brownian motion. These fluctuations occur on a length scale similar to the size of the colloids. This random motion thereby causes the colloids to settle into the contact line.

In contrast to this, the length scale of bacterial movement is in the magnitude of $10\mu m$ - an order of magnitude bigger than the random Brownian motion [2]. Such a displacement allows bacteria to leave the contact line after entering, or to move over the perimeter of the contact line. This is illustrated in panel (c) of Figure 6.8.

Figure 6.8 shows the deposition patterns at different times relative to their evaporation time, $t_{evaporation}$. Panels (a) and (b) show the deposition pattern of the water drop that has been analyzed in section 6.1 at $0.1t_{evaporation}$ and $1t_{evaporation}$. Panels (c), (d) and (e) show the pattern of motile E.Coli bacteria at $0.1t_{evaporation}$, $0.5t_{evaporation}$, and $1t_{evaporation}$ respectively. Finally, panels (f), (g) and (h) show the pattern of non-motile E.Coli bacteria at $0.2t_{evaporation}$, $0.25t_{evaporation}$ and $0.375t_{evaporation}$.

At early times in drop evaporation, when capillary flow towards the contact line is still small, bacteria seem to settle into the contact line only by being stuck at the contact line, either at the wedge-shaped liquid-vapor-solid interface or between other bacteria. They may either move in place in an attempt to propagate, or may cease movement.

At later times in drop evaporation, when the capillary flow towards the contact line increases asymptotically, bacteria show little to no self-generated movement, thereby settle into the contact line as passive tracers. After evaporation, the contact line shows a structure similar to what has been observed in the pattern of colloidal particles in a buffer drop.

However, a difference with the pattern of passive colloids can be discerned. It was assumed that the structure of the colloids arises from the clusters that move into the contact line. This occurs as well for the immobilized bacteria, but is not the only effect. Several bacteria stop movement before entering the bulk of the contact line, which is shown in panel (e) of Figure 6.8. As can be seen, several bacteria are lodged in place.

This observation is similar to observations in previous research (Dombrowski et al., 2004). The narrow region at the contact line shaped like a wedge with decreasing angle (Popov, 2005). This has been shown to lock bacteria into place (Dombrowski et al., 2004). However, (Dombrowski et al., 2004) also suggests that bacteria are trapped by the initially accumulated bacteria, thereby suggesting that a biofilm is formed.

[2] This value can be calculated theoretically from the duration and velocity of E.Coli runs ($1s$ and $10\mu m/s$, respectively, observed from bacteria trajectories, or deduced from the velocity plot.

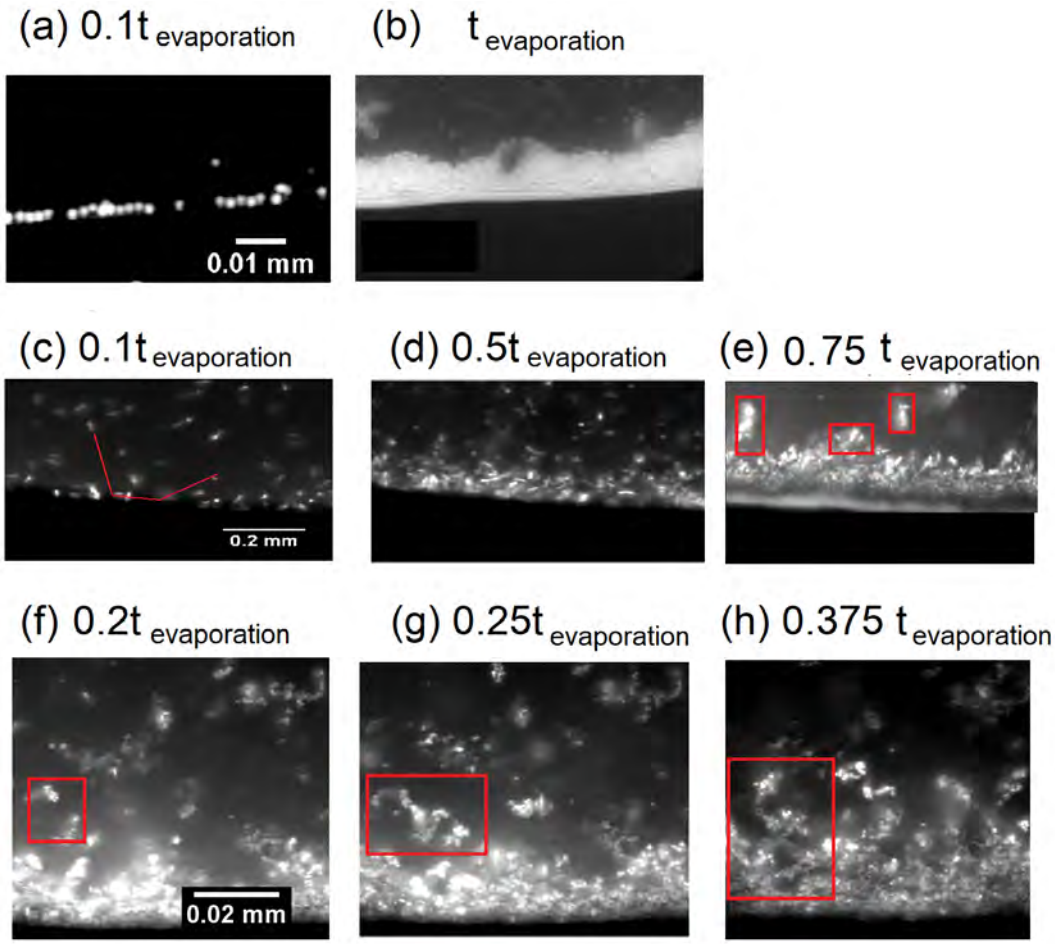

FIGURE 6.8: Contact line deposition within a drop of water containing $0.1w\%$ colloids (top), and a drop of motility buffer containing CONC motile (middle) or CONC non-motile (bottom) E.Coli strain at subsequent times indicated relative to the evaporation times $t_{evaporation}$ of ten, twenty and twelve minutes, respectively. The red lines in panel (c) indicate a bacteria's movement through the contact line. The red boxes in panel (e) show several motile bacteria that stop moving before entering the contact line The red boxes in panels (f-h) indicate a growing cluster of non-motile bacteria.

This formation of a biofilm may be confirmed by our observation of bacteria being stuck between other bacteria or stuck before reaching the contact line deposition. However, further understanding of biofilm nucleation is required to validate such statements.

Before turning to the non-motile bacteria, it may prove useful to summarize findings on motile bacteria.

In short, the motile E.Coli bacteria observed in the evaporating drop show a high motility. A number of bacteria move out of the contact line, instead of settling into the deposition pattern.

However, E.Coli motility decreases after about half the evaporation time. After this critical time, bacteria seem to move only due to random Brownian motion and

due to the capillary flow. Their radial velocity increases over time while the tangential velocity remains approximately equal, similar to what has been observed with colloids.

In other words, the motile bacteria seem to behave as passive tracers after a critical time. A number of bacteria stops movement towards the contact line before reaching the accumulated deposition.

6.4 Non-motile E.Coli bacteria

The non-motile bacteria oscillate randomly due to Brownian motion. The bacteria have been observed to coalesce into random clusters upon collision. Subsequently, small clusters grow when additional bacteria stick. When compared to single bacteria, these clusters have a bigger size that results in a smaller Brownian motion. In addition, larger particles are not dragged along with the flow as small tracers.

In other words, these clusters mostly remain in place and form an obtrusion to measurements. Figure 6.9 shows three ways in which this occurs. First, their presence hinders observation with GDPT. For example, consider the bacterial trajectory indicated by the red lines. Due to the neighbouring cluster, it cannot be traced by GDPT. Second, the clusters form a physical obstacle for other bacteria moving towards the contact line. This has an effect on the flow that arises, which is the third obtrusion. The presence of the cluster indicated by the blue box seems to divert the flow as indicated in green.

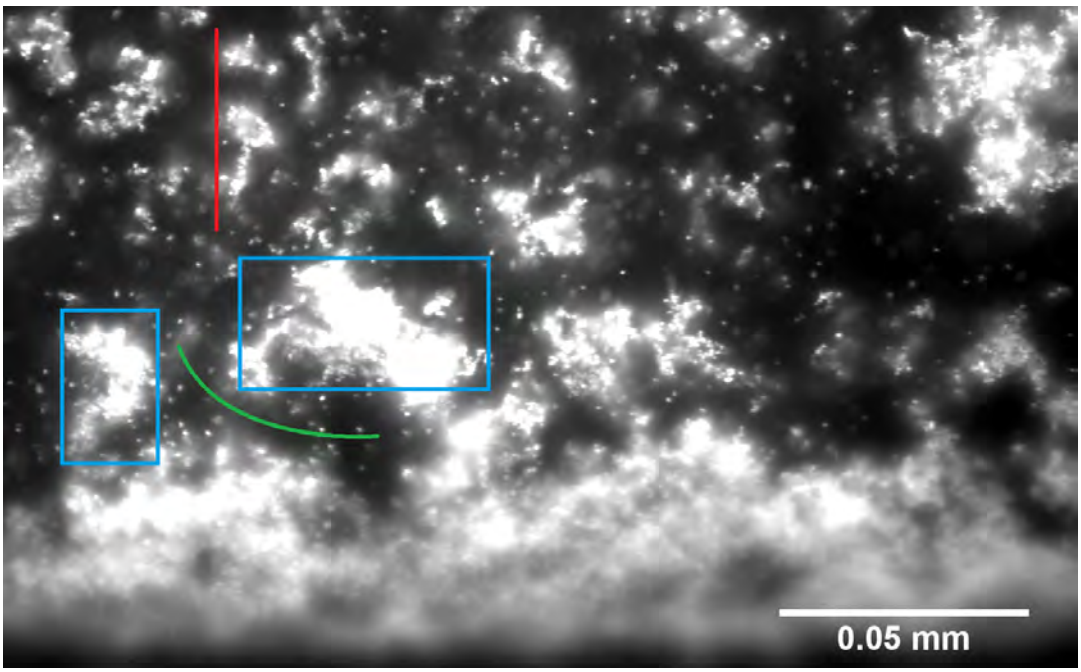

FIGURE 6.9: GFP fluorescent image with $40x$ magnification of deposition pattern of non-motile E.Coli strain during drop evaporation showing large structure formation (blue) of clustering bacteria. These structures disable GDPT analysis, since bacteria neighbouring these clusters cannot be observed (red). Furthermore, they act as boundaries that seem to alter the flow (green).

Two additional qualitative observations can be made from the image material. First, the contact line seems to be dragged inward, suggesting the occurrence of a

strong inward flow at the end of the evaporation time. Figure 6.9 shows the contact line deposition at frame 3478 (a) and frame 3604 (b). As can be seen, the deposited bacteria are dragged inward, indicated by the increased distance to the contact line. Second, the fluorescent signal of bacteria decreases over time. As such, the contact line slowly fades away. A similar observation has been made with the motile E.Coli strain.

Chapter 7

Discussion

This chapter serves three purposes. First, it discusses to what extend we have succeeded in answering our research question. Second, it discusses what shortcomings or limitation in the research can be improved upon. Third and finally, this chapter concludes with suggestions for promising questions to explore in the future.

The goal of this research has been to investigate how self-propelling E.Coli bacteria deposit in an evaporating sessile drop with pinned contact line.

Observations of previous papers have been reproduced first. In short, the radially outward velocity in a drop of water containing colloidal particles has been shown to increase over time. The deposition pattern has shown a transition from ordered to disordered packed particles. Experiments on colloidal particles in a motility buffer solution have shown additional irregularities in the contact line deposition and the potential occurrence of additional flows.

Experiments have indicated that the motility of E.Coli in the evaporating drops can be categorized into two phases. Initially, bacteria can move out of the contact line. In the end, bacteria act as passive tracers of which a number stops movement towards the contact line before reaching the contact line deposition. Finally, non-motile E.Coli bacteria have been shown to coalesce more than passive colloids, showing an effect of the nontrivial chemical makeup of E.Coli bacteria.

In the previous chapter, we observed that both the swimming velocity and the fluorescence of the bacteria was decreasing over time. This decrease posed a severe limitation to the experiments because it was not possible to investigate bacterial motility during the rush-hour phenomenon.

Bacterial motility may decrease due to the formation of a biofilm or cell damage leading to cell death. Biofilm formation is expected to occur only in the last minutes of evaporation, which is later than the decrease in motility is observed. Therefore, investigational efforts are directed only at cell damage. From a small literature review and experimental observations, it is expected that cell damage can occur due to (1) a lack of resources; (2) increased salt concentration; (3)cytotoxicity of GFP; or (4) overexposure by the light source. Each of these will be discussed below.

The lack of nutrients in the motility buffer means that bacteria have a limited life-time. However, it can be argued that the duration of time spent in the buffer is not the cause of motility decrease observed in the experiments. Experiments taken several hours apart show a similar initial motility and decrease in motility during evaporation.

Experiments taken a day later show a decreased initial motility, showing the effect of the limited life-time of bacterial cultures in the motility buffer [1]. This observation further disproves the formation of a biofilm that reduces motility.

However, this decrease is smaller than the steep decline of motility towards Brownian levels that is observed in our experiments. As such, it may be concluded that the decrease of motility within an experiment is not only due to the simple lack of resources.

Increased salt concentration as a cause of cell damage in bacterial colonies has been reported in many biological research papers (sources). This injury results from dehydration due to the osmotic pressure difference between the environment and the inside of the cell. Specifically, a salt concentration increase to 10% has an impact on cell integrity (hajmeer2006impact, metris2014metabolic).

In our experiments, the $NaCl$ motility buffer solution has an initial salt concentration of $0.067M$, corresponding to $3.914g/L$ or roughly 0.4%. Towards the end of evaporation, crystals form and the concentration nears 100%.

This increase is not homogeneous across the drop due to the inhomogeneous evaporation rate. Since this rate is highest near the contact line – the region of interest – it may increase above critical values earlier than elsewhere in the drop. The diffusion time of $Na+$ and $Cl-$ ions, $O(10^3 s)$, is much larger than the evaporation time, indicating that the higher increase in concentration near the contact line does not lower due to diffusion. Evidently, it is necessary to calculate analytically how the concentration increases across the drop over time or to experimentally compare the contact line and drop center regions.

Experiments on varying (lower) salt concentrations can be performed to determine if bacteria remain fluorescent and motile for a longer period of time. However, the initial salt concentration has a lower limit determined by the osmotic pressure. This pressure is directed inwards if the salt concentration of the fluid is too low. This drives fluid into the bacteria, causing them to swell or even burst (Wood).

Investigating the effect of different salt concentrations on bacterial motility and fitness however did not fit the scope of this research.

Further, it may prove of interest to determine if bacteria are dead or only dehydrated in order to understand the final stage of deposition pattern formation. To this end, a drop of growth medium can be pipetted to the formed stain. If bacteria resume dividing and again emit fluorescent light, they have survived the drop evaporation.

The fluorescent signal results from excitation of the green-fluorescent protein (GFP) that the E.Coli excrete (Zimmer, 2002). For the decrease in fluorescence to occur, GFP production must have stopped and GFP already present must be exhausted after excitation. This may occur when bacteria die during evaporation. GDPT protein may fluoresce after the death of the bacterial host. However, it may depleted over time by emitting light.

To investigate the effect of overexposure, a trial measurement has been performed. Two drops of a single culture have been exposed to a different amount of light. The test measurement was illuminated continuously, while the second measurement was illuminated only $5s$ every minute. The moment in time at which the outer perimeter of the contact line fades away has been observed to shift. For the

[1] This occurs when storing the culture in the fridge, but also when storing it in room temperature.

test measurement, it occurs at one third of the evaporation time, whereas it occurs at the end of evaporation for the second measurement.

In other words, these measurements have hinted that the fluorescent signal remains longer if the bacteria are illuminated less during evaporation. A similar experiment with the motile E.Coli strain needs to be performed to determine whether overexposure causes only a decrease in fluorescent signal or also a decrease in motility.

Various papers have reported that the green-fluorescent protein (GFP) has a detrimental effect on the health of bacteria (ansari2016cellular, liu1999green). Other papers have argued against this observation (zimmer2002green).

If GFP is a cause of bacterial cell damage, using it as tracer has severe implications for experiments on E.Coli motility in evaporating sessile drops. However, it lies outside of this research to investigate the potential detrimental effect of GFP on E.Coli.

The GDPT software tracks individual particles and appears to be more difficult in use if particle concentration increases. Therefore, it may not be the most appropriate tool to assess particle motion in the contact line region, which has been shown to be of particular interest to determine the deposition pattern of bacteria. To improve upon this, an increase in frame rate to $30fps$ and increase in resolution, to determine individual bacteria more reliably, may be required.

A switch to Particle Image Velocimetry (PIV) may be opted for if individual bacteria cannot be discerned and if the research question focuses on the collective behavior of bacterial. A downside of PIV is that it does not track individual bacteria.

The camera's maximum frame rate is not reached in current measurements due to data processing limitations of the connection the camera makes with the computer. The frame rate is limited to $4f/s$ for the entire FOV. A FOV of 400x400 pixels is required to obtain the frame rate of $16f/s$. This data limitation imposes a trade-off between FOV size and frame rate. From a first approximation, it appears that a frame rate of $4fps$ is sufficient to observe under $40x$ magnification the movement of motile E.Coli with a the typical velocity of $10\mu m/s$. Therefore, measurements have been performed with a frame rate of $4fps$, for which the camera's full FOV can be used.

However, analysis by the GDPT software depends on frame rate, as well as particle velocity, illumination quality and the amount of particles. In the GDPT software, movement of particles cannot be observed if the relation between these three factors is inadequate: for example if the velocity is too high; the frame rate too low; the amount of particles too high; or a combination of these factors.

In terms of these factors, the experiments performed in this research were suboptimal. For example, a high number of motile bacteria is visible in the raw images but is not analyzed correctly. As such, improvements and additional measurements are required.

This research has hinted to interesting behavior of motile and non-motile E.Coli bacteria in the configuration of an evaporating sessile drop with pinned contact line. These observations can be validated with further research, but also point to interesting new research.

In particular, the movement of bacteria in the contact line region has been shown to be of interest. The interaction of various components can be investigated in more detail. For example, to what extent is movement in the contact line caused by the

individual bacterium, by hydrodynamic interaction between neighbouring bacteria, or by the mean flow? When bacteria do not tumble and as such do not reorient themselves individually, are they still capable of leaving the contact line? This may show whether or not the motion of individual bacteria is a significant factor in contact line movement.

Chapter 8

Conclusion

This research set out to investigate how the deposition pattern in evaporating drops is affected by the motility of the particles. In particular, the motion and deposition of motile E.Coli bacteria has been compared to that of passive colloidal particles in an evaporating drop of water that deposit in a ring-stain due to the radially outward capillary flow.

The first two sets of test measurements were performed on passive colloidal particles in a drop of water and in a drop of motility buffer solution. The purpose of these test measurements is to account for observations that may occur in the buffer drop of bacteria that are not caused by bacterial movement.

Initial measurements on the drop of water have reproduced findings from previous research, showing the capillary flow and ring-shaped stain with a transition from ordered pattern to disordered packing. The following measurements on passive colloids in a drop of buffer solution have shown two different deviations from this test measurement with water drops. It has been shown that a homogeneous deposition pattern of colloids is formed when a recirculating flow occurs which has been hypothesized to arise from a surface tension gradient. It has also been shown that in the buffer solution the colloids cluster more frequently, leading to a ring-shaped stain with structural irregularity. Both of these effects have been hypothesized to arise from the nonzero salt concentration in the buffer solution. When compared to passive colloids, the high motility of motile E.Coli bacteria has shown to lead to a slower growth of the contact line deposit. Observations indicate that bacteria have a propensity to leave the contact line.

The motility and fluorescent signal of bacteria has been shown to decrease over time, causing the bacteria to act as passive tracers before the 'rush hour' phenomenon sets in. These now-passive bacteria then deposit into the contact line stain similarly to the colloids in the buffer solution, leading to a stain with structural irregularities.

a number of experiments have not yet been analyzed with sufficiently low amount of outliers due to difficulties in the analysis software caused by the high concentration of motile bacteria and insufficient frame rate and illumination quality

Due to the decrease in bacterial velocity, it has not been possible to investigate the trade-off between high radially outward velocity and bacterial motions. The conditions in which bacteria colonies die may be investigated to attempt these measurements. However, the contact line behavior of bacteria has been shown to an interesting venture for investigation.

Despite the experimental difficulties posed by bacteria as test subject, this research has shown the deposition pattern of motile E.Coli bacteria in evaporating drops and has hinted to intriguing differences with established frameworks of passive colloidal particles. The bacteria can move out of the contact line region unless

trapped in or before the contact line deposition and act as passive tracers after a critical time.

Bibliography

Barnkob, Rune, Christian J. Kahler, and Massimiliano Rossi (2015). "General defocusing particle tracking". In: *Lab on a Chip* 15.17, pp. 3556–3560. ISSN: 14730189. DOI: 10.1039/c5lc00562k.

Deegan, R. D. et al. (1997a). "Capillary flow as the cause of ring stains from dried liquid drops". In: *Nature* 389, pp. 827–829.

— (2000). "Contact line deposits in an evaporating drop". In: *The American Physical Society* 62.1, p. 756.

Deegan, Robert D et al. (1997b). "Capillary flow as the cause of ring stains from dried liquid drops". In: *Nature* 389.6653, p. 827.

Dombrowski, Christopher et al. (2004). "Self-concentration and large-scale coherence in bacterial dynamics". In: *Physical review letters* 93.9, p. 098103.

Hocking, LM (1983). "The spreading of a thin drop by gravity and capillarity". In: *The Quarterly Journal of Mechanics and Applied Mathematics* 36.1, pp. 55–69.

Hu, H. and R.G. Larson (2002). "Evaporation of a sessile droplet on a substrate". In: *Journal of physical chemistry* 106, pp. 1334–1344.

— (2005). "Analysis of the Microfluid Flow in an Evaporating Sessile Drop". In: *Langmuir* 21, pp. 3963–3971.

Islam, MA (2004). "Einstein–Smoluchowski diffusion equation: a discussion". In: *Physica Scripta* 70.2-3, p. 120.

Jaijus, Pallippadan Johny and Anugrah Singh (2010). "Flow visualization and solute transport in evaporating droplets". In: *AIChE journal* 56.7, pp. 1674–1683.

Kasyap, T. V., D. L. Koch, and M. Wu (2014a). "Bacterial collective motion near the contact line of an evaporating sessile drop". In: *Physics of fluids* 26, p. 111703.

Kasyap, TV and Donald L Koch (2012). "Chemotaxis driven instability of a confined bacterial suspension". In: *Physical review letters* 108.3, p. 038101.

Kasyap, TV, Donald L Koch, and Mingming Wu (2014b). "Bacterial collective motion near the contact line of an evaporating sessile drop". In: *Physics of Fluids* 26.11, p. 111703.

Koch, D. and G. Subramanian (2011). "Collective hydrodynamics of swimming microorganisms: living fluids". In: *Annual Review of Fluid Mechanics* 43, pp. 637–659.

Lauge, E. and T.R. Powers (2009). "The hydrodynamics of swimming microorganisms". In: *Reports on progress in physics* 72, pp. 1–36.

Li, Shuoqi et al. (2018). "Dynamics of viscous entrapped saturated zones in partially wetted porous media". In: *Transport in Porous Media* 125.2, pp. 193–210.

Marin, A. G. et al. (2011). "Order-to-Disorder Transition in Ring-Shaped Colloidal Stains". In: *American Physical Society* 107, p. 085502.

Oron, A., S.H. Davis, and S.G. Bankoff (1997). "Long-scale evolution of thin liquid films". In: *Reviews of Modern Physics* 69, pp. 931–980.

Parsa, Maryam, Souad Harmand, and Khellil Sefiane (2018). "Mechanisms of pattern formation from dried sessile drops". In: *Advances in colloid and interface science* 254, pp. 22–47.

Popov, Y.O. (2005). "Evaporative deposition patterns: Spatial dimensions of the deposit". In: *Physical Review* 71, p. 036313.

Rapp, Bastian E (2016). *Microfluidics: Modeling, Mechanics and Mathematics*. William Andrew.

Schwarz-Linek, Jana et al. (2016). "Escherichia coli as a model active colloid: A practical introduction". In: *Colloids and Surfaces B: Biointerfaces* 137, pp. 2–16.

Still, Tim, Peter J Yunker, and Arjun G Yodh (2012). "Surfactant-induced Marangoni eddies alter the coffee-rings of evaporating colloidal drops". In: *Langmuir* 28.11, pp. 4984–4988.

Yeomans, Julia M, Dmitri O Pushkin, and Henry Shum (2014). "An introduction to the hydrodynamics of swimming microorganisms". In: *The European Physical Journal Special Topics* 223.9, pp. 1771–1785.

Zimmer, Marc (2002). "Green fluorescent protein (GFP): applications, structure, and related photophysical behavior". In: *Chemical reviews* 102.3, pp. 759–782.